Journal of Materials Chemistry B

Accepted Manuscript

ROYAL SOCIETY OF CHEMISTRY

www.rsc.org/materialsB

Upconversion Nanocomposites for Photo-based Cancer Theranostics

Shuailiang Wang [a], Anyao Bi [a], Wenbin Zeng *[a], Zhen Cheng *[b]

[a] *School of Pharmaceutical Sciences, Central South University, 172 Tongzipo Road, Changsha, 410013, PR China.*

[b] *Molecular Imaging Program at Stanford (MIPS), Canary Center at Stanford for Cancer Early Detection, Department of Radiology and Bio-X Program, School of Medicine, Stanford University, California, USA.*

* *Corresponding author: E-mail address: wbzeng@hotmail.com (W. Zeng), zcheng@stanford.edu (Z. Cheng).*

Abstract Lanthanide ions doped upconversion nanoparticles (UCNPs) are known to be able to convert the long-wavelength excitation light (usually 980 nm) into high-energy ultraviolet (UV) or visible emissions, and they have attracted significant attentions because of their distinct photochemical properties including sharp emission bands, low autofluorescence, high tissue penetration depth, inert to ambient interference and minimized photodamage to tissues. Untill now, UCNPs have shown great potentials in various realms including bioimaging, biosensing and biomedical applications. Especially in recent years, UCNPs based nanocomposites have been found to be promising tools for multi-modal imaging and low-invasive photo-based therapy of tumors. In this review, we summarize the recent achievement and progress of UCNPs based multifunctional nanoplatforms for bioimaging and cancer phototheranostics, including photodynamic therapy (PDT) and photothermal therapy (PTT). Furthermore, some emerging trends, future directions as well as challenges in this rapidly growing field are discussed.

Contents

1. Introduction

Cancer is known to be one of the most serious diseases that has threatened human health in recent decades because of uncontrolled growth of cancer cells and the possibility of metastasis, and cancer treatment has always been one of the very central themes of clinical problems.[1] Traditional chemotherapy and radiotherapy usually bring great suffer to patients and often have no curative effect to metastatic tumor. In order to prevail in the battle against cancer, novel treatment strategies with higher therapeutic effect and less side-effect are in urgent need. Very recently, the development of low-invasive cancer treatments has attracted significant attentions, especially photo-based cancer theranostic regimens including photodynamic therapy (PDT), photothermal therapy (PTT) and photo-induced drug delivery.[2] Cancer theranostic is a new research field to integrate imaging and therapy of cancer, which can simultaneously report the presence and status of tumor as well provide therapeutic effect,[3] and PDT is one of the most frequently used therapy strategies in cancer theranostics. As known, a typical PDT process contains three vital components: excitation light, photosensitizer (PS) and molecule oxygen. Traditional PDT usually selects high-energy ultraviolet (UV) or visible light as energy donor. Under the irradiation of excitation light, PS molecules are boosted from ground state to excited state with higher energy. Consequently, molecule oxygen can accept the energy originate from excited PS molecules, leading to the generation of singlet oxygen and other reactive oxygen species (ROS). Finally, ROS species are able to disrupt neighboring cancer cells through cell apoptosis and anti-angiogenesis effects.[4]

Importantly, PDT possesses a remarkable advantage over chemotherapy and radiotherapy which commonly cause significant side-effect due to their poor-selectivity. Through selectively illuminating specified tumor region, PDT leaves those noncancerous tissues unaffected and results minimal side-effect to patients.[5] However, in traditional PDT, PS molecules are typically excited by short-wavelength UV or visible light which has limited penetration depth in biological tissues, thus limiting the extensive applications of PDT on internal or large tumors.[4] Near infrared (NIR) light (700-1000 nm) has demonstrated to have much stronger tissue penetration ability, and therefore NIR light excited PDT could partially overcome such a limitation. Furthermore, the low-energy NIR light falls into the 'transparency window' of biological tissues, and it normally has no harm to tissues since water and blood cells can hardly absorb any NIR light.[6]

The development of rare-earth (Ln^{3+}) doped upconversion nanoparticles (UCNPs) has provided unprecedented opportunities for the realization of NIR triggered PDT. It has been demonstrated that the trivalent lanthanide ions own partially occupied 4f orbits under the shield of outer 5s and 5p shells. Therefore under the NIR light excitation (usually 980 nm), rare earth doped UCNPs are able to absorb the energy of two or more excitation photons and transform into the excited status that possesses higher energy to fulfil the upconversion luminescence (UCL) process. Subsequently, NIR, visible or even UV light emission can be observed.[7,8] The UCL mechanisms have been well studied and can be primarily categorized into five classes: (a) excited state absorption (ESA), (b) energy transfer upconversion (ETU), (c) photon avalanche (PA), (d) cooperative energy transfer (CET), and (e) energy migration-mediated upconversion (EMU), as shown in Fig. 1.[9] Because of its intrinsic properties, lanthanide-doped UCNPs display many distinct advantages such as sharp emission bands, low background autofluorescence, high photostability and minimal photo-damage to living organisms. Meanwhile, the long-wavelength excitation light has much stronger tissue penetrate ability compared with UV or visible light, thus it is much more compatible for photo-induced cancer theranostics.[10] Untill now, UCNPs have exhibited many potential applications in various biological areas including

bioimaging,[11] biosening[12], and biometric fingerprint recognition.[13] Thanks to the rapid development of nanoscience and nanotechnology, high quality UCNPs with tunable morphology and size as well as emission bands have been readily available nowadays.[14] It is convenient and reliable to prepare UCNPs based nanocomposites for cancer phototheranostics. In this review, we summarize recent developments and achievements of UCNPs based bioimaging and cancer theranostics. Particularly, UCNPs and their nanocomposites based PDT, PTT and synergistic cancer phototheranostic strategies are discussed in detail. Additionally, some emerging trends and future efforts as well as challenges toward this rapidly growing field are discussed in this review.

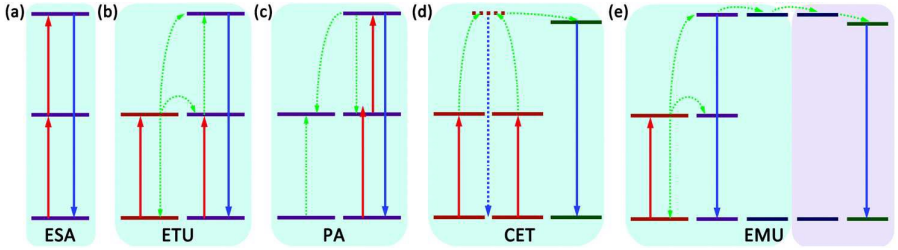

Fig. 1 Schematic illustration of UCL mechanisms, (a) excited state absorption (ESA), (b) energy transfer upconversion (ETU), (c) photon avalanche (PA), (d) cooperative energy transfer (CET), and (e) energy migration-mediated upconversion (EMU). (Reprinted with permission from ref. 9. Copyright 2015, Royal Society of Chemistry).

2. Fabrication of UCNPs-based nanocomposites for cancer phototheranostics

Ideally UCNPs based nanocomposites for cancer phototheranostics should satisfy several criteria including efficient UCL emission and high biocompatibility, meanwhile, enough stability was requisite to confront the complicated *in vivo* environment. Plenty of preparation and modification strategies to fabricate high quality UCNPs based nanocomposites have been developed and applied extensively in recent years, as will be described in the Section 2.1, 2.2 and 2.3.

2.1 Synthesis of high quality UCNPs

Generally, lanthanide doped UCNPs contain three important constituents, *i.e.*, the host matrixes, the sensitizers and the activators. Different kinds of host matrixes provide luminescence centers with different coordination numbers, energy transfer distances, and different energy transfer efficiencies.[15] Till now, types of host matrixes have been applied including CaF_2,[16] LaF_3,[17] $LiYF_4$,[18] YF_3,[19] $KGdF_4$,[20] $KMnF_3$,[21] $NaYF_4$,[22] $NaGdF_4$,[23] $NaLuF_4$,[24] amongst these typically used matrixes, $NaREF_4$ (RE = Ln, Sc and Y) matrixes are most extensively used due to their excellent photochemical stability and relatively low phonon energy.[25] The sensitizer applied in UCNPs to enhance the UCL emission should have excited energy levels located in the NIR region, also they have large absorption cross-sections and energy levels matched well with the activators. Yb^{3+} has been demonstrated to be the most suitable sensitizer because of its simple energy levels (only one excited state $^2F_{5/2}$) and large absorption cross-section at 980 nm ($^2F_{7/2}$-$^2F_{5/2}$) that match well with those most frequently used activators Er, Tm and Ho. Due to their ladder-like energy level arrangement, these activator ions are able to absorb more than one excitation photons (980 nm) and consequently emitting one photon with higher energy and shorter wavelength during the relaxation process.[26] Er doped UCNPs are able to emit 525 nm ($^2H_{11/2}\rightarrow{}^4I_{15/2}$), 540 nm ($^4S_{3/2}\rightarrow{}^4I_{15/2}$), and 660 nm ($^4F_{9/2}\rightarrow{}^4I_{15/2}$) fluorescence with high UCL efficiency. As to Tm doped UCNPs, the emission can occupy the spectrum from UV to NIR range, including 290 nm ($^1I_6\rightarrow{}^3H_6$), 345 nm ($^1I_6\rightarrow{}^3F_4$), 362 nm ($^1D_2\rightarrow{}^3H_6$), 450 nm ($^1D_2\rightarrow{}^3F_4$), 475 nm ($^1G_4\rightarrow{}^3H_6$), 644 nm ($^1G_4\rightarrow{}^3F_4$) and 803 nm ($^3H_4\rightarrow{}^3H_6$) (See Fig. 2).[9]

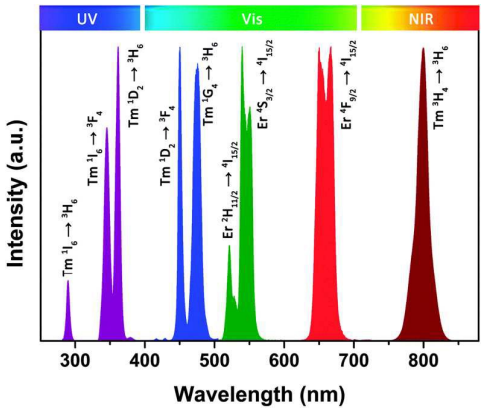

Fig. 2 Representative UCL emission bands ranged from UV to NIR regions of Yb-Er and Yb-Tm doped UCNPs under 980 nm excitation. (Reprinted with permission from ref. 9. Copyright 2015, Royal Society of Chemistry).

$NaREF_4$ UCNPs are known to possess two different kinds of crystalline structures, *i.e.*, cubic phase (α-phase) and hexagonal phase (β-phase). It has been demonstrated that the UCL efficiency of β-phase UCNPs are at least one order higher than UCNPs of α-phase.[27] Therefore, preparation of UCNPs with hexagonal phase is quite significant to fabricate ideal nanocomposites for cancer phototheranostics. Until now, a variety of synthesis procedures have been developed for the preparation of β-phase UCNPs, including thermal decomposition method, hydro(solvo)thermal method, co-precipitation method, ionic liquid method and dual phase method, as has been comprehensively discussed in several previous reviews.[28-30]

Among these synthesis strategies, hydrothermal and thermal decomposition methods are two of the most frequently used strategies to fabricate hydrophobic UCNPs with uniform morphology, pure-phase, tunable diameters and UCL emission bands. For instance, Liu et al. have established thermal decomposition protocols for the fabrication of core-shell $NaGdF_4$ and $NaYF_4$ UCNPs. They indicate that the average diameter and morphology of as-prepared UCNPs can be adjusted through the variation of experimental compositions (Table 1), and mono-dispersed UCNPs with uniform diameter and morphology can be easily achieved.[31] Li and coworkers have applied solvothermal strategies for one-pot preparation of PAA-capped water-soluble β-$NaYF_4$ UCNPs for bioimaging.[32] Moreover, different kinds of other metal ions can

be doped in UCNPs to adjust the intensity of different UCL emission bands.[33] For instance, Zhao and coworkers demonstrate that the corporation of Mn^{2+} in $NaYF_4$: Yb, Er UCNPs selectively enhances the red emission through cross-relaxation mechanisms.[34] Soon after, Kim et al. indicate that Fe^{3+} doping into the $NaGdF_4$: Yb, Er nanocrystals enhances the overall UCL intensity at both 540 nm and 660 nm. A maximum enhancement can be observed with 30 mol % Fe^{3+} doping, and the red and green emission can be enhanced by 30 and 34 times respectively, which can be attributed to the broken local crystal field symmetry around the activators (Er^{3+}) that favors the hypersensitive transitions.[35] Furthermore, Li^+ Ca^{2+}, or Zn^{2+} doping could also fine-tune the UCL emission of various kinds of UCNPs.[36-38]

Table 1: Typical experimental settings for the preparation of UCNPs of varying compositions.

UCNPs	OA/ODE (v/v mL)	Fluoride/RE ratio	Morphology	Average size (nm)
$NaGdF_4$: Yb/Tm/Y (49/1/20%)	4/6	3.9	Sphere	22
$NaYF_4$: Yb/Tm (29/1%)	3/7	4	Sphere	18
$NaYF_4$: Yb/Tm (49/1%)	3/7	4	Sphere	26
$NaYF_4$: Yb/Tm (49/1%)@ $NaYF_4$	3/7	4	Rod	43 × 26

Importantly, green synthesis of UCNPs plays critical role for the fabrication of eligible nanoparticles for in vivo applications. For instance, Hu et al. reported a simple "green" solvothermal strategy for the first time.[39] Through the application of DEG/EG/water as mix solvent at elevated temperature (300 ^oC), PEI-coated water soluble UCNPs with a diameter of 5 nm and bright luminescence are prepared, meanwhile, the nanoparticles are highly crystallined with hexagonal $NaYF_4$ structure. As traditional method usually needed laborious heating and multistep post-treatment, this one-pot "green" synthesis procedure is both facile and applicable, thus is highly significant for the preparation of super-small sized UCNPs with strong upconversion luminescence and excellent biocompatibility.

2.2 Modification strategies of UCNPs

Normally, UCNPs synthesized through the two most frequently used strategies are capped by oleate or oleylamine,[40,41] rendering them have poor solubility in aqueous solution. For biomedical application, UCNPs must be water-soluble and biocompatible, thus the surface modification of UCNPs is highly significant for further fabrication of UCNPs based nanocomposites for cancer phototheranostics. Typically, hydrophobic UCNPs can be converted into hydrophilic through several well-studied methods that can be mainly categorized into four groups:[42] (1) direct modification of the hydrophobic capping ligands; (2) bilayer coating with amphiphilic polymers or molecules; (3) extra layer or shell addition; and (4) complete replacement of the original hydrophobic capping ligands. Since these methods have been comprehensively summarized in previous reviews,[6,10,25] we will only briefly introduce some of the most representative methods here.

Typically, direct modification refers to the oxidation of unsaturated carbon-carbon double bonds of oleate or oleylamine, leading to the formation of carboxyl or epoxy groups. As reported by Huang and coworkers,[43] the unsaturated carbon bonds can be oxidized by Lemieux-von Rudloff reagent to provide bare carboxyl groups. Thus the solubility of as-prepared UCNPs is dramatically improved and renders them available to conjugate with other molecules for further biomedical applications. Furthermore, ozone and 3-chloroperoxy-benzoic acid have also been applied for the oxidation of unsaturated carbon-carbon bonds.[44,45] Bilayer coating with amphiphilic polymers or molecules is also one of the most used strategies to improve the dispersibility of hydrophobic UCNPs in aqueous solution. Oleate or oleylamine capped UCNPs normally are decorated with long alkyl chain, thus other amphiphilic molecules or polymers containing long alkyl chains can be stabilized on the surfaces of UCNPs through Van-der-Waals interactions to render them water soluble. Till now, various kinds of amphiphilic molecules or polymers have been applied for UCNPs modification including poly (ethylene glycol) (PEG) incorporated phospholipids

(PLs)[46], long alkyl chain modified poly (acrylic acid) (PAA),[47] chitosan[48] and different kinds of Tween.[49,50] For instance, Zhao et al. fabricate Tween-20 modified $NaYbF_4$: Tm, Gd@$NaGdF_4$ UCNPs with good water-dispersibility and strong blue-emitting as photosensitizer (hypocrellin A, HA) carriers for PDT of cancer cells.[51] Chang and coworkers apply amphiphilic lipid polymer (RGD-PMAO-DOPE) coated UCNPs as NIR remote controlled transducer for simultaneous photodynamic therapy and cell imaging of MC540 cells.[52] The addition of an extra layer or shell is another regularly used process to render UCNPs water-soluble. Generally, the growing of silica shell or noble metal (Ag or Au) shell on the surface of UCNPs could satisfy such requirements. For example, Shi et al. construct S-nitrosothiol (R-SNO)-grafted mesoporous silica coated UCNPs mesoporous silica coated UCNPs as an intelligent X-ray-controlled NO-releasing upconversion nanotheranostic system for on-demand depth-independent hypoxic radiosensitization.[53] Liu et al. established multi-functional naonparticles (UCNP@Fe_3O_4@Au) coated with Au shell and further modified by PEG and anti-HER2 antibody for specified detection and simultaneously localized PTT of Cancer Cells.[54] Complete replacement of the original hydrophobic ligands, known as ligand exchange, is the most studied modification strategy of UCNPs. For direct (one-step) ligand exchange, PAA,[55] PEG[56] and dimercaptosuccinic acid (DMSA)[57] are several of the most used surfactants. As to two-step ligand exchange, hydrophobic UCNPs are typically processed with strong acid or nitrosonium tetrafluoroborate ($NOBF_4$) to render them ligand-free,[58,59] further attachment of other surfactants makes them water-dispersible and equips with necessary active chemical groups.

2.3 Fabrication of UCNPs-based nanocomposites

Normally, UCNPs modified through the above-mentioned methods are water-dispersible and available to further conjugation with other molecules (anti-cancer drugs, target or PS molecules) for cancer phototheranostics and other numerous biomedical and bioanalytical applications.[60] On one hand, several PS

molecules, drugs and functional nanomaterials can be loaded into UCNPs through the physical adsorption or electrostatic attraction mechanisms. For example, Liu's group fabricates UCNPs coated by PEG@2×PEI through layer-by-layer method, lipophilic PS molecules Chlorin e6 (Ce6) can be loaded on UCNPs through hydrophobic interactions, furthermore, negatively charged siRNA can be adsorbed on positively charged UCNPs due to the PEI layer coating.[61] UCNPs nanocomposites prepared through the above-mentioned procedure possesses the combination of PDT and gene therapy capacity. As a result, under a 980 nm NIR excitation, real-time tracking and synergistic cancer therapeutic effect can be observed in their study. In another experiment, Wang et al. construct a FRET system between UCNPs and gold nanoparticles (Au NPs) for the simple and sensitive turn-on detection of biothiols. The citrate ions capped AuNPs are negatively charged, thus they are able to adsorbed onto the surface of CTAB modified UCNPs which are positively charged. Due to the surface plasmon absorption of AuNPs, green emission of UCNPs is quenched, whereas the addition of biothiols lead to the aggregation of AuNPs and restores fluorescence of UCNPs.[62]

On the other hand, PS molecules or organic dyes can be encapsulated into the mesoporous silica shell coated UCNPs. For instance, Zhang et al. construct mesoporous silica coated UCNPs encapsulating a combination of zinc (II) phthalocyanine (ZnPc) and merocyanine 540 (MC540) for simultaneous activation of two photosensitizers by single excitation for enhanced PDT.[63] Wu and coworkers prepare mesoporous silica coated UCNPs that are loaded with anticancer drug doxorubicin (DOX) and further grafted with ruthenium complex to act as photoactive molecular valves. Such UCNPs-based nanocomposites are able to release DOX under a 0.35 W cm^{-2} excitation (974 nm) which is under the certain threshold of maximum permissible exposure intensity of skin (0.726 W cm^{-2}), thus this strategy is highly compatible to biological samples with minimized overheating and photodamage.[64]

Thirdly, covalent conjugation is another frequently used strategy for the preparation of UCNPs-based nanocomposites. Since physical adsorption and encapsulation method usually suffers serious leakage of PS molecules into the circulation system,

leading to reduced therapeutic effect, covalent conjugation provides an alternative pathway to prepare nanocomposites with higher stability. Besides, covalent conjugation method normally owns higher loading capacity of PS molecules or other molecules. For example, J. Krull et al. prepare OA-capped UCNPs which are further modified with o-phosphorylethanolamine by ligand exchange and consequently conjugated with a photocleavable o-nitrobenzyl-5-fluorouracil (ONB-5-FU) prodrug for NIR triggered anticancer drug release.[65] Upon excitation with 980 nm NIR laser, Tm^{3+} doped UCNPs are able to emit UV lights, thus the ONB group undergoes photolytic cleavage and free 5-FU is released, up to 77% release of drug compared with direct UV illumination can be observed within 10-15 min irradiation. Meanwhile, controlled release of 5-FU can be manipulated through the adjustment of NIR irradiation power. Huang's group prepares organic dye conjugated UCNPs for the ratiometric imaging of intracellular pH values. Organic dye xylenol orange (XO) is conjugated on the surface on UCNPs *via* the formation of amide bond between SiO_2-NH_2 modified UCNPs and carboxyl groups of XO molecules under the assist of EDC and NHS. Such nanocomposites can act as sensitive UCL pH probes both in PBS solution and living cells with high stability and low cytotoxicity.[66]

3. UCNPs-based nanocomposites for tumor imaging

Since traditionally used fluorophores (including fluorescent dyes or proteins and fluorescent beads) for *in vivo* optical imaging usually exist several intrinsic disadvantages such as short wavelength excitation induced overheat and photodamage, low penetration depth, severe photobleaching and autofluorescence that led to low signal-to-noise ratio (SNR), thus limiting their applications especially in deeper tissue imaging. As a new generation of imaging agents, on the contrary, UCNPs are normally excited by NIR light (usually 980 nm) which is located in the transparent region of tissues, thus has minimum autofluorescence and photodamage. Meanwhile, the penetration depth of NIR light is much deeper than short-wavelength UV or

visible light, the high photostability renders them applicable for long-term monitoring of cell-tracking or the distribution of drugs.[67] Particularly, Gd^{3+} and Yb^{3+}/Lu^{3+} doped UCNPs have been successfully applied as MRI and CT contrast agents for *in vivo* biomedical imaging, meanwhile, radiolabeled (for instance, ^{18}F, ^{124}I and ^{153}Sm) UCNPs can be applied in PET/SPECT imaging realms.[68] Also, UCNPs could be conjugated with targeting molecules including antibodies and receptors for tumor targeted imaging.[69,70]

3.1 UCL imaging

Since it has been demonstrated that UCNPs possess full spectrum emission under single wavelength excitation,[71] meanwhile, the UCL emission can be fine-tuned from visible to NIR regions,[72,73] thus UCNPs are promising optical bioimaging probes for both *in vitro* and *in vivo* applications. Till now, two types of the most used UCNPs, *i.e.*, the Tm^{3+} doped blue/NIR emitting UCNPs and Er^{3+} doped green/red emitting UCNPs have been extensively used in the optical imaging of various kinds of biosamples and biospecimens. Furthermore, UCNPs can be labeled or conjugated with antibodies, small molecules such as FA, peptides such as RGD and other targeting agents for tumor targeted UCL imaging.

Multicolor imaging is an important tool that allows simultaneous visualizing several events under a single snapshot with reduced reagents and minimized sampling errors.[74] Although Er^{3+} doped UCNPs are able to emit multicolor (green and red) under single excitation, the application of Er^{3+} and Tm^{3+} co-doped UCNPs in multicolor imaging is restricted by the serious cross-relaxation which could induce compromised or even quenched blue emission from Tm^{3+}. In an interesting experiment, Huang's group[74] has prepared Er^{3+} doped UCNPs encapsulated with grafted cationic conjugated polyelectrolyte brushes (PFNBr) that own dual-upconversion emission properties for multicolor imaging of cancer cells. PFNBr is an efficient two photon absorption (TPA) fluorescent material which possesses enhanced water-solubility and photophysical properties compared with traditional

linear conjugated polyelectrolytes (CPEs). Herein, PFNBr acts as a surfactant to present on the surface of OA-coated UCNPs to render such nanocomposites highly water-soluble. Due to the Er^{3+} doping, green and red emissions are observed under a 980 nm laser excitation, while PFNBr is able to emit blue fluorescence under an 800 nm laser excitation. Importantly, the UCL intensities of all emissions remain almost unchanged after 30 min of continuous wavelength (CW) excitation, making such dual-upconversion nanocomposites applicable multicolor imaging probes for cancer cells. As demonstrated by *in vitro* assessments with HepG-2 cells, blue emission can be observed under an 800 nm excitation, meanwhile, green and red fluorescence can also be observed under a 980 nm excitation. Moreover, fluorescent images under different channels demonstrate that there is no FRET between the RGB emissions. Furthermore, fluorescence can be observed in the cellular cytoplasm indicating efficient internalization of $NaYF_4$:Yb-Er@PFNBr in HepG-2 cells. Such UCNPs based nanocomposites provide promising candidates for the fabrication of efficient multicolor imaging probes.

Besides multicolor imaging, UCNPs can be applied to tumor targeted UCL imaging. For instance, in 2009, Li and coworkers report c-RGD conjugated UCNPs for tumor targeted imaging.[75] In their experiment, OA-capped UCNPs are primarily transformed into water-soluble with Lemieux-von Rudloff reagent and further modified with PEG-NH_2. Subsequently, c(RGDFK), an well known polypeptide which has high affinity with $\alpha_v\beta_3$ integrin receptor that normally expressed on the surface of cancer cells and tumor neovasculature, is coated on the surface of UCNPs to act as the targeting agent (as shown in Fig. 3a). To investigate the targeting ability of UCNPs-RGD, MCF-7 (low integrin $\alpha_v\beta_3$ expression) and U87MG (high integrin $\alpha_v\beta_3$ expression) cell lines have been chosen and incubated with UCNPs-RGD. Strong green and red fluorescence can be observed under 980 nm excitation within U87MG cells without auto-fluorescence, while in MCF-7 cells, only very weak fluorescence is noticed, indicating the specificity of UCNPs-RGD to cancer cells with high integrin $\alpha_v\beta_3$ expression (see Fig. 3b). *In vivo* imaging experiments with U87MG tumor and MCF-7 tumor dual-bearing mice also demonstrate the targeting ability of

UCNPs-RGD (see Fig. 3c). Under the continuous wavelength excitation of 980 nm NIR light, Tm^{3+} doped UCNPs is able to emit 803 nm NIR light, as demonstrated by EMCCD camera, intense NIR fluorescence signals can be observed on the region of U87MG tumor, while in the region of MCF-7 tumor, no significant UCL signal is noticed. Meanwhile, a high signal-to-noise ratio (about 24) is observed between the tumor region and the background, indicating that UCNPs conjugated with targeting molecules can be highly promising probes for tumor targeted UCL imaging.

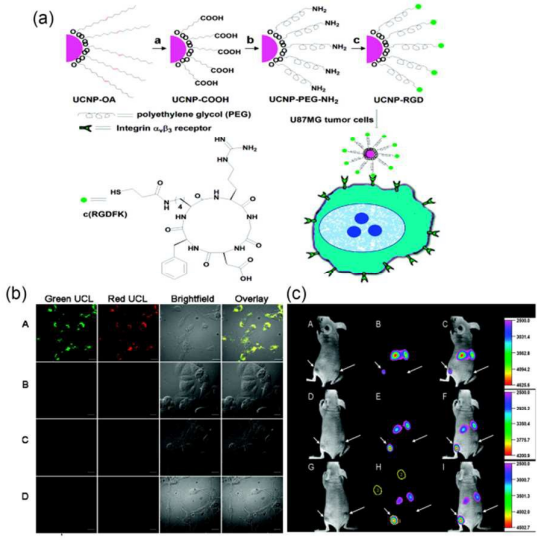

Fig. 3 (a) Schematic illustration of the synthetic procedure of UCNPs-RGD. (b) Confocal UCL images of U87MG cells (A) and MCF-7 cells (B) incubated with UCNPs-RGD (37 ^{o}C, 30 min), U87 MG cells incubated with UCNPs-PEG-NH_2 (C) and UCNPs-RGD in the presence of unlabeled c(RGDFK) (D) at 37 ^{o}C. (c) Time dependent *in vivo* UCL imaging of U87MG tumor and MCF-7 tumor dual-bear nude mice after intravenous injection of UCNPs-RGD over a 24 h period. (Adapted with permission from ref. 75. Copyright 2009, American Chemical Society).

However, for *in vivo* UCL imaging application, the power and irradiation time of 980 nm laser should be precisely controlled to minimize the inevitable overheat effect induced by long-time continuous wavelength irradiation. To eliminate the overheat effect, UCL imaging probes based on 915 nm and 808 nm lasers excited UCNPs have been fabricated by He et al. in 2011 and Yan et al. in 2013.[76,77] Since water and biological specimens have strong absorption of 980 nm NIR light, thus restricted its

penetration depth for the *in vivo* imaging application, and even worse induced local overheat. An alternative irradiation of 915 nm could well settle such problem due to the much weaker absorption of water, thus it could bring about enhanced penetration depth and reduced overheat effect. While the 808 nm excited UCNPs applies novel sensitizer groups, *i.e.*, Nd^{3+}-Yb^{3+}, to sensitize the activators doped in UCNPs to avoid the strong absorption of water at 980nm. Both *in vitro* and *in vivo* heating effect induced by irradiation have been investigated, 808 nm laser is found to have much lower heat effect compared with the 980 nm excitation. Meanwhile, except the visible UCL emission from activators doped in UCNPs, such nanoparticles also exhibit intense NIR emission from Yb^{3+} (980 nm, $^2F_{5/2}\rightarrow{}^2F_{7/2}$) as well as down-shifting luminescence emissions from Nd^{3+} at 1064 nm ($^4F_{3/2}\rightarrow{}^4I_{13/2}$) and 1532 nm ($^4I_{13/2}\rightarrow{}^4I_{15/2}$), such novel luminescence properties render Nd^{3+}/Yb^{3+} doped UCNPs meaningful dual-channel probe for *in vivo* imaging under a single excitation.

As discussed above, rare earth doped UCNPs provide meaningful alternatives to traditional organic dyes for *in vivo* bioimaging due to their intrinsic advantages including low background fluorescence, sharp emission bands and enhanced penetration depth. Meanwhile, the exploration of 808 nm and 915 nm excited UCNPs have the potential to overcome the latent overheat effect induced by 980 nm laser excitation, thus further expanding their use for *in vivo* application. Furthermore, UCNPs based nanocompostites for other imaging strategies besides the UCL optical imaging have also been fabricated and demonstrated in recent years, as will be summarized below.

3.2 Photoacoustic imaging

Photoacoustic imaging (PAI), which often relied on the usage of the photoacoustic (PA) effect, has been considered to be a powerful tool for noninvasive structural and functional imaging with good spatial resolution and penetration ability.[78] Recently, NIR activated PAI for deep tissue imaging has aroused tremendous attention due to its minimized background interference and enhanced contrast of PA images. Rare earth

doped UCNPs have emerged as potential agents for optical imaging *in vitro* and *in vivo* imaging.[79,80] However, UCNPs always suffer luminescence quenching in aqueous solution and generate abundant thermal energy owing to the solvent relaxation process, which are usually considered as drawbacks of UCNPs for *in vivo* imaging. Interestingly, Zhao and his team have taken advantage of the heating capacity of UCNPs to generate enhanced PA signals for *in vivo* PAI under NIR excitation (see Fig. 4a).[81] Hydrophobic UCNPs are transformed into water-soluble through the formation of inclusion complex with α-cyclodextrin (α-CD). As-prepared UC-α-CD nanoparticles are highly dispersible in aqueous solution without obvious morphological or size alteration. Compared with OA-UCNPs dispersed in cyclohexane, the UCL efficiency of UC-α-CD dispersed in water is dramatically decreased by ~ 62%. According to the luminescence quenching, they anticipate that the corresponding thermal expansion could induce enhanced PA signals,[82] which has been demonstrated by subsequent experiments. The PA signals of OA-UCNPs in cyclohexane, UC-α-CD dispersed in water and distilled water as blank control are recorded under the 980 nm excitation, respectively. Both the OA-UCNPs dispersed in cyclohexane and distilled water show negligible PA signals, while UC-α-CD dispersed in water exhibited excellent PA signals, as further demonstrated with a tissue mimicking phantom (Fig. 4b and 4c). *In vivo* PA imaging with a severe combined immunodeficiency (SCID) female mouse also shows clear contrast enhancement within 35 min post injection of UC-α-CD. Such UCNPs based nanocomposites possess several advantages including easily handled, high photostability, strong penetration ability, low background interferences and negligible cytotoxicity even under high concentration, rendering UC-α-CD an attractive PA contrast agent for biomedical imaging.

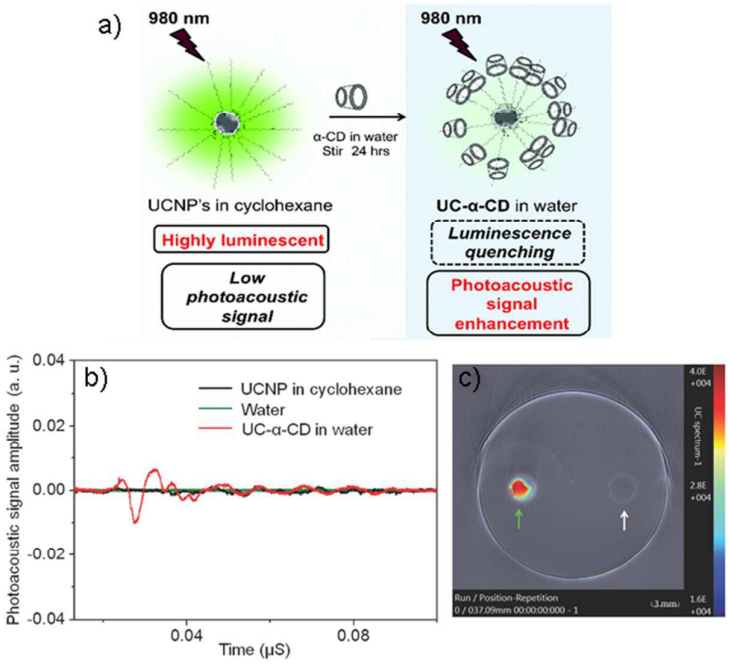

Fig. 4 (a) Schematic illustration of UCL quenching induced PA signal enhancement of UC-α-CD in water. (b) High resolution PA signals generated from UCNPs in cyclohexane (black curve, 1 mg/mL), UC-α-CD in water (red curve, 1 mg/mL) and distilled water (green curve) under 980 nm excitation. (c) PA section image of tissue-mimicking phantom containing channels filled with UC-α-CD in water (green arrow) and distilled water (white arrow). (Adapted with permission from ref. 81. Copyright 2014, Wiley-VCH Verlag GmbH & Co. KGaA).

3.3 Multi-modal imaging

Besides the optical imaging, recently developed biomedical imaging strategies could satisfy the requirements of structural or functional imaging of biological systems, including those most popular imaging modalities such as magnetic resonance imaging (MRI), computed tomography (CT), positron emission tomography (PET) and single-photon emission computed tomography (SPECT). However, none of individual of these "newfashioned" imaging strategies could give comprehensive information for biomedical imaging.[3] To overcome the defects of single imaging modality and harness the combined merits of these imaging strategies, significant efforts have been devoted to the fabrication of multimodal imaging probes. UCNPs have shown unparalleled advantages in optical imaging and could provide much higher sensitivity and spatial

resolution than radiological imaging modalities. However, UCL optical imaging lacks the capability to achieve anatomical details.[30] Thus, UCNPs based nanocomposites integrate the UCL imaging and other radiological imaging strategies for multi-modal *in vivo* imaging could become important tools for clinical diagnostics and biomedical research.[83-85]

MRI is known to have excellent spatial resolution and exceptional ability to achieve anatomical details as well as good penetration depth for *in vivo* imaging, but suffer intrinsic disadvantages including limited sensitivity.[30] The combination of MRI and UCL optical imaging for bimodal *in vivo* imaging could address such problems through the improvement of desired sensitivity and resolution. UCNPs-based nanoprobes for UCL/MR bimodal imaging have been well studied and many successful probes have been synthesized.[86-88] For instance, for the first time, Shi and coworkers has prepared UCNPs based dual-targeting nanoprobe ANG/PEG-UCNPs according to the receptor-mediated transcytosis (RMT) for simultaneous *in vivo* MR/UCL imaging of glioblastoma.[89] First of all, they synthesize OA-capped monodispersed $NaYF_4$:20%Yb/2%Tm/15%Gd@$NaGdF_4$ UCNPs, herein, Gd^{3+} is doped to promote the formation of ultrasmall $NaYF_4$: Yb/Tm/Gd core. Meanwhile, a layer of ultrathin $NaGdF_4$ shell is coated to enhance the UCL intensity as well to facilitate its utility as a MRI contrast agent (CA). Consequently, as-prepared UCNPs have been processed with hydrochloric acid (HCl) and further capped with aminepoly(ethylene glycol)-thiol (NH_2-PEG5k-SH) to form PEG-UCNPs. After that, Angiopep-2 (ANG, TFFYGGSRGKRNNFKTEEY) is decorated on UCNPs through covalent conjugation to act as a dual-targeting agent due to its special binding ability to the low density lipoprotein receptor related protein (LRP), which has been demonstrated to be overexpressed on both glioblastoma cells and BBB. As a result, ANG/PEG-UCNPs have relative high uptake ratio in glioblastoma cells through the BBB-crossing transcytosis. Compared with the clinical used fluorescent imaging agent 5-ALA for brain tumor surgery, the strong blue emission (Tm^{3+}: 448 nm, $^1D_2 \rightarrow {}^3F_4$; 476 nm, $^1G_4 \rightarrow {}^3H_6$) of ANG/PEG-UCNPs is still noticeable under a 5 mm-thick pork obstruction, indicating the remarkable penetrate ability of NIR excitation (980

nm). After intravenous injection of ANG/PEG-UCNPs, T1-weighted MRI at different time points indicates that the contrast of glioblastoma in the targeting group is significantly enhanced. Furthermore, the average T1-weighted MR signal intensity of the tumor region is enhanced by ~ 81.3% at 1h post-injection, which is much higher than clinical used contrast agent Gd-DTPA (a maximum enhancement of 15.2% in 10 min post-injection). Meanwhile, the boundary of tumor region is much more clearly delineated than that of Gd-DTPA. Furthermore, the *in vivo* blood circulation half-time of ANG/PEG-UCNPs is up to 72.4 min due to the PEGylation, thus the MR contrast could maintain strong enough for a relative long period (more than 2 hours). Histological/hematological examination indicates that ANG/PEG-UCNPs are highly biocompatible to brains with negligible *in vivo* toxicity. Such UCNPs-based nanoprobes have great potential for glioblastoma diagnosis and intraoperative positioning of tumors to maximum the accuracy of surgical resection.

UCNPs with high proportion doping of Yb^{3+} or Lu^{3+} could be used as CT contrast agent, as has been reported by several groups.[90-92] MRI is known to be highly suit for soft tissue examination, while CT is more proper for bone, lung and chest imaging and also cancer detection.[30] Thus, the combination of MRI, CT and UCL imaging no doubt provides more comprehensive information of tissues. An ideal UCL/CT/MR imaging agent should meet several criteria including bright UCL emission, excellent X-ray absorption coefficient and high MR signal intensity enhancement. Till now, several successful nanoprobes based on UCNPs for UCL/CT/MR tri-modal imaging have been fabricated.[93-96] For example, in 2014, Shi et al. present the first nanoprobe based on Ho^{3+} doped UCNPs for T2 weighted MRI and simultaneous UCL/CT imaging of tumors without fluorescent quenching (Fig. 5a).[97] Ho^{3+} is one of the most frequently used activitors in UCNPs, the short electronic relaxation time as well as highly effective magnetic moment render it owns the most efficient T2 relaxation than other supermagnetic lanthanide ions, therefore, Ho^{3+} doped UCNPs are able to integrate the T2-MR and UCL imaging abilities into one single nanoparticle (see Fig. 5c-5g). Furthermore, they indicate that Yb^{3+} and Ho^{3+} own higher attenuation characteristics than the clinical used CT contrast agent iobitridol, thus Ho^{3+} doped

$NaYbF_4$ UCNPs provide high-resolution 3D anatomic supplementation to UCL/MR imaging to fulfill biomedical imaging requirements. In their experiments, Ho^{3+} doped UCNPs are further modified with biocompatible DSPE-PEG2000-NH_2 to improve the water dispersibility of UCNPs. The high-performance T2-MRI is carried out through intravenous injection of Lipo-UCNPs to glioblastoma-bearing mice. The tumor region can be clearly imaged for over 2 h, and the average signal intensity (SI) of tumor is remarkably reduced to a maximal ≈ 75.3% at 1.5 h post-injection due to the enhanced permeability and retention (EPR) effect induced accumulation of Lipo-UCNPs at the tumor region. Furthermore, the strong green emission due to Ho^{3+} doping ($^5F_4$, $^5S_2 \rightarrow {}^5I_8$) under a 980 nm excitation makes such Lipo-UCNPs available for *in vivo* UCL imaging. Moreover, *in vivo* CT imaging is implemented through intravenous injecting Lipo-UCNPs to mice at timed intervals. An immediate signal enhancement of heart can be observed for more than 30 min period. The signal enhancement of spleen and liver lasts to almost 2 h post-injection. Compared with iobitridol which owns short circulation time and can hardly accumulate at heart, spleen and liver, Lipo-UCNPs have relative long-lasting time in blood circulation with high concentration, thus they are much more suitable for liver tumor CT imaging. Furthermore, *in vitro* and *in vivo* toxicity assessments indicate that Lipo-UCNPs hardly cause any acute or chronic toxicity, thus Lipo-UCNPs are highly significant to act as contrast agents for multi-modal *in vivo* imaging applications.

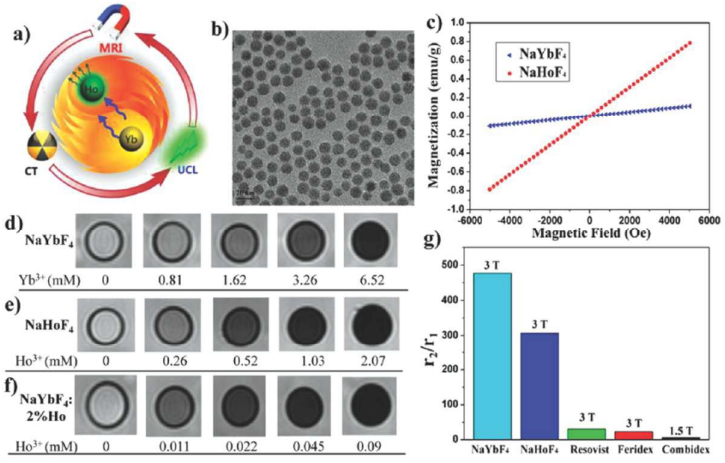

Fig. 5 a) Schematic illustration of Ho^{3+}-doped UCNPs as the T2-MRI/UCL/CT tri-modal imaging probes. b) TEM images of $NaHoF_4$ UCNPs dispersed in chloroform. c) M–H curves of $NaYbF_4$ and $NaHoF_4$ NPs at 300 K. T2

-weighted phantom MR images of d) Lipo-$NaYbF_4$, e) Lipo-$NaHoF_4$, and f) Lipo-UCNPs at different concentrations. g) Comparison of r2/r1 values among the clinical negative CAs and the Ho^{3+}/Yb^{3+}-based NPs. (Reprinted with permission from ref. 97. Copyright 2014, Wiley-VCH Verlag GmbH & Co. KGaA).

UCNPs could also be combined with the new generation of non-invasive nuclear imaging strategies including PET and SPECT which could provide three-dimensional functional images. For instance, Song et al. construct dimeric cyclic RGDyk ($(cRGDyk)_2$) peptide conjugated $NaGdF_4$:Yb^{3+}/Er^{3+} UCNPs which is further labeled with ^{124}I (denoted as ^{124}I-$c(RGDyk)_2$-UCNPs) for UCL/MR/PET tri-modal specific-targeted imaging of tumor angiogenesis.[98] In another experiment, Li and coworkers prepare $NaLuF_4$:Yb,Tm core UCNPs which further grows a shell of $^{153}Sm^{3+}$-doped $NaGdF_4$ as a four-modal nanoprobe (denoted as NaLuF4:Yb,Tm@$NaGdF_4$(^{153}Sm)) for *in vivo* UCL/CT/MR/SPECT imaging of tumor angiogenesis.[99] In several earlier experiments, Li's group has also fabricated ^{18}F-labeled UCNPs as contrast agent for PET/MRI/UCL *in vivo* imaging.[100,101] Very recently, as a combination of frequently used imaging strategies, F. Lovell's group successfully fabricated Porphyrin-Phospholipid-Coated UCNPs for hexamodal imaging.[102] The porphyrin-phospholipid (PoP) coating renders UCNPs available for fluorescence (FL) and photoacoustic (PA) imaging. Meanwhile, the PoP-UCNPs are endowed with PET and Cerenkov luminescence (CL) imaging ability through further incubation with ^{64}Cu. Furthermore, combined with the intrinsic UCL and CT imaging ability of Tm^{3+} and high content Yb^{3+} doped UCNPs, PoP-UCNPs are qualified as hexamodal imaging probes. *In vitro* and *in vivo* experiments indicated such nanocomposites highly potential for FL/PA/PET/CT/CL/UCL hexamodal imaging although the long-term toxicity of PoP-UCNPs need further assessment. According to these successful trials and meaningful achievements, we conclude that UCNPs based nanocomposites are promising contrast agents for multi-modal *in vitro* and *in vivo* imaging of tumors in future explorations.

4. UCNPs-based nanocomposites for cancer phototheranostics

As has been discussed above, UCNPs based nanocomposites can be useful tool for single or multi modal imaging. After deliberate decoration and modification, UCNPs can serve as promising carriers of drugs and PS molecules. By combining the strong UCL emissions under the 980 nm laser excitation, UCNPs can also be applied in the area of photo-based drug delivery and therapy. Until now, different therapeutic strategies have been developed by using the ample UCL emission of UCNPs. Furthermore, combined with the multi-modal imaging ability, such UCNPs based nanocomposites can be highly significant phototheranostic probes for cancer as well as other diseases.

4.1 PDT

As an emerging strategy for the treatment of various kinds of diseases, PDT has been demonstrated to be highly powerful in the realm of cancer therapy.[4] However, traditional PDT is restricted to the treatment of superficial tumors due to the poor penetration ability of the typically used visible excitation light. Since UCNPs are able to transform NIR excitation light into UV or visible emission to activate neighbouring PS molecules, as mentioned above, and the NIR excitation light is known to have much deeper penetration depth,[6] UCNPs loaded with PS molecules are much more promising for the treatment of large and deep-seated tumors.

UCNPs are known to have multiple emission bands in the range from UV to NIR region. Both the blue emission of Tm^{3+} and green/red emissions from Er^{3+} have been explored for PDT in recent years. For instance, in 2013, Zhao et al. take advantage of Tm^{3+} doped UCNPs conjugated with photosensitizer hypocrellin A (HA) for NIR triggered PDT of cancer cells.[51] In their experiment, Tm^{3+} doped $NaYF_4$ UCNPs are prepared and further modified with Tween-20 to improve its hydrophilicity as well capability to load PS molecules. HA is loaded on the surface of UCNPs through

hydrophobic-hydrophobic interactions with a loading amount of 0.01 mmol g^{-1}. As described above, Tm^{3+} doped UCNPs are able to emit blue light (475 nm, $^1G_4 \rightarrow {}^3H_6$) under 980 nm NIR excitation to activate HA molecules and consequently produce singlet oxygen to kill cancer cells. The cell viability of both A549 and HeLa cells can be significantly affected by such nanocpmposite under the 980 nm excitation, indicating HA conjugated UCNPs are highly potential for PDT of cancer cells. Meanwhile, due to the Gd^{3+} doping in the shell layer, such nanocomposites are able to act as T1 contrast agent for MRI, which has also been demonstrated in their experiments. Along the increase of UCNPs concentration, T1-weighted images can be brightened and enhanced r1 value of water protons can be also observed. Furthermore, the Yb^{3+} doping also endows such nanocomposites the ability to act as CT contrast agent due to its high atomic number and strong X-ray attenuation. Such nanocomposites hold the capability of simultaneous PDT and multimodal imaging, thus they are important for photo-based cancer theranostics. Not only the blue emission from Tm^{3+}, green/red emissions of Er^{3+} can also be used to activate PS molecules for *in vivo* PDT of tumor. For instance, in 2014, Chen et al. prepare monodisperse $LiYF_4$: Yb/Er UCNPs with different diameters, and they further load PS molecules ZnPc-COOH through electrostatically coupling to form the UCNP-ZnPc-COOH PDT system (see Fig. 6a).[103] The energy transfer efficacy between UCNPs and ZnPc-COOH is calculated to be 96.3% due to the direct conjugation of PS molecules on UCNPs. A cell viability of larger than 95% is observed at 1 mg mL^{-1} of UCNPs-ZnPc-COOH indicating its high biocompatibility. *In vitro* PDT with MDA-MB-231 cells confirms that UCNPs-ZnPc-COOH has increased cytotoxicity under a 980 nm excitation. Meanwhile, compared with conventional PDT use 660 nm red excitation to activate ZnPc molecules, the 980 nm excitation has deeper tissue penetration, the PDT effect of UCNPs-ZnPc-COOH can be observed even under a 10 mm tissue phantom. Furthermore, larger UCNPs (diameter 47 nm) are demonstrated to have higher PDT efficacy than smaller counterparts, as shown in Fig. 6b. Further *in vivo* PDT experiment is conducted through the use of H22 tumor-bearing mice, 20 min of irradiation under 980 nm (0.5

W cm^{-2}) is implemented at 12 h post-injection (intratumorally) of 30 μL of UCNPs-ZnPc-COOH (0.5 mg mL^{-1}). After a period of 2 weeks, the tumor volumes of mice received PDT treatment change from ~ 240 mm^3 to ~ 501 mm^3 while the control group (without laser) increases remarkably to ~ 1282 mm^3 (see Fig. 6c). Bodyweight analysis and other histological analysis of tumor tissues also demonstrate the high therapeutic efficacy of UCNPs-ZnPc-COOH under the 980 nm excitation (Fig. 6d). Moreover, UCNPs-ZnPc-COOH can also be utilized for UCL imaging of cancer cells. After incubation with ZnPc-COOH, the red emission of UCNPs is nearly quenched, while the green emission (540 nm) is reserved and can be utilized to monitor cancer cells. Thus such nanocomposites can act as imaging-guided PDT agents for NIR triggered cancer theranostics.

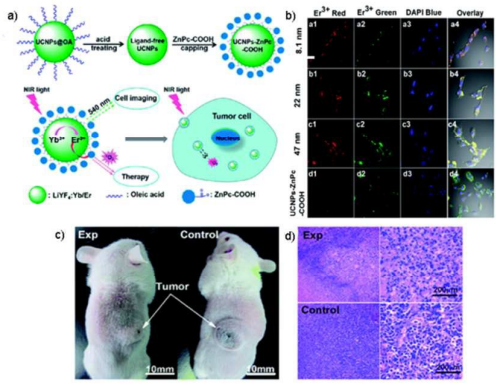

Fig. 6 (a) Schematic illustration of multifunctional $LiYF_4$: Yb/Er UCNPs for cancer theranostics. (b) Confocal laser scanning microscopy images of MDA-MB-231 cells after incubation with different size $LiYF_4$: Yb/Er UCNPs and UCNP-ZnPc-COOH for 2 h at 37 °C. (c) Therapeutic effects of mice in experimental and control groups after 14 days, respectively. (d) Images (left) and the corresponding high-resolution images (right) of H&E stained tumor tissues harvested from the experimental and control groups after 14 days. (Adapted with permission from ref. 103. Copyright 2014, Royal Society of Chemistry).

The PDT efficacy can be improved through dual-photosensitizer loading strategies, as been reported by Zhang and coworkers in 2012. Two different kinds of PS molecules zinc (II) phthalocyanine (ZnPc) and merocyanine 540 (MC540) are loaded on mesoporous silica coated $NaYF_4$: Yb, Er UCNPs.[63] Since the emission of UCNPs

at 540 nm and 660 nm are well overlapped with absorption bands of MC540 and ZnPc, respectively, both of the emission bands are harnessed to activate PS molecules to produce cytotoxic singlet oxygen for the treatment of cancer cells (see Fig. 7a and 7b). Such nanocomposites are expected to have higher PDT efficacy than mono-loaded UCNPs. As having been demonstrated by *in vitro* PDT experiments, the dual-loading UCNPs have much higher singlet oxygen production and superior cell-killing efficiency compared with mono-photosensitizer (MC540 or ZnPc) loaded UCNPs, as shown in Fig. 7c. Further *in vivo* PDT for melanoma tumor bearing mice are carried out after intravenous injection of PS loaded UCNPs with subsequent NIR excitation at 4 h post-injection. Compared with control groups, the growth speed of tumor is significantly retarded after 6 d and 8 d treatment (see Fig. 7d to 7f). Such nanocomposites provide a combined strategy that gives amplified therapeutic efficacy under single excitation and are highly potential to act as non-invasive cancer theranostic platforms.

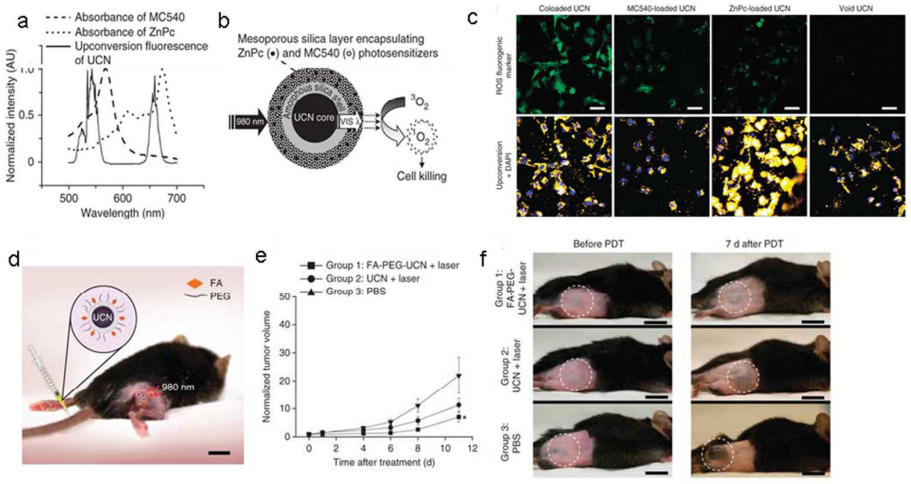

Fig. 7 (a) The UCL spectrum of the UCN and the absorption spectra of ZnPc and MC540 photosensitizers. (b) Schematic illustration of mesoporous-silica-coated UCNs co-loaded with ZnPc and MC540 photosensitizers for PDT (not to scale). (c) Evaluation of ROS generated in cells treated with differentially loaded UCNs and then exposed to NIR laser (2.5 W/cm2 for 40 min). (d) Schematic diagram showing UCN-based targeted PDT in a mouse model of melanoma intravenously injected with UCNs surface modified with folic acid (FA) and PEG moieties. Scale bar, 10 mm. (e) Change in tumor size as a function of time after treatment to assess the effectiveness of UCN-based mediated targeted PDT in tumor-bearing mice intravenously injected with

FA-PEG-UCNs. (f) Representative gross photos of a mouse from each group 1-3 before (0 d) and 7 d after PDT treatment. Scale bars, 10 mm. (Adapted with permission from ref. 63. Copyright 2012, Nature Publishing Groups).

However, it has been demonstrated that water has relative strong absorption at 980 nm region, which could induce overheating and photodamage of tissue, or worse, lower the PDT efficiency. Very recently, Zhu et al. prepare Nd^{3+} doped UCNPs that can be excited at 808 nm where water has minimized absorption to resolve above mentioned problems.[104] In their experiment, UCNPs are doped with Nd^{3+} and Yb^{3+} to form the Nd^{3+}→Yb^{3+}→activator system that can be excited at 808 nm and modified with 2-aminoethyl dihydrogen phosphate (AEP). Er^{3+} is selected as activator and the 660 nm ($^4F_{9/2} \rightarrow {}^4I_{15/2}$) red emission is harnessed to activate PS molecules Chlorin e6 (Ce6) covalently conjugated on UCNPs. Such nanoparticles are further modified with FA-PEG-COOH to improve its water dispersibility and cancer-targeting ability. Two kinds of cancer cells KB and A549 cells are utilized to confirm the targeting ability of as-prepared UCNPs. *In vitro* imaging demonstrates that UCNPs can enter folate receptor expressed KB cells through folate receptor-mediated endocytosis, while UCNPs can hardly enter folate receptor negative A549 cells, indicating the selectivity of FA-PEG-Ce6-UCNPs to folate receptor positive cancer cell lines. The 808 nm excitation also renders such nanocomposties to have deeper penetration depth than 980 nm excited UCNPs. As introduced in their experiment, when a pork tissue of 8 mm thickness is covered on the UCNPs samples, the singlet oxygen production of 808 nm and 976 nm excitations are 17.2% and 3.6%, respectively. Moreover, upon 808 nm excitation, FA-PEG-Ce6-UCNPs are still able to produce singlet oxygen even under a 15 mm thickness pork muscle tissue. Furthermore, no obvious cell viability alteration under a 30 min exposure to 808 nm can be observed, indicating its dark toxicity. *In vitro* PDT experiments indicate that the PDT efficiency of FA-PEG-Ce6-UCNPs is time-dependent and concentration-dependent for folate receptor positive cell lines (KB cells). As to folate receptor negative A549 cells, effective cell killing ability can be also observed due to the non-receptor-mediated cellular uptake. Nanocomposites fabricated through such strategies can possess highly

improved PDT efficacy of deep-seated tumors with higher biocompatibility.

PDT based on UCNPs nanocomposites show great potential for the non-invasive treatment of tumors with elevated penetration ability. Compared with traditional PDT strategies, UCNPs based PDT can not only provide therapeutic effect of tumors in deeper region, but also present various precise imaging information of tumors, thus it is much more convenient and meaningful for preoperative diagnostic and intraoperative location of tumor. In this rapidly progressed realm, novel strategies to achieve elevated therapeutic efficiency for large and internal tumors are very important, furthermore, the long-term biosafety of such UCNPs based nanocomposites for PDT is in urgent need.

4.2 PTT

Photothermal therapy has been regarded as an alternative medical strategy to conventional cancer treatments such as surgery, radiotherapy, and chemotherapy. PTT utilizes photoabsorbers to generate heat from laser illumination and lead to thermal ablation of cancer cells. In recent years, various nanomaterials with high NIR light absorbance such as gold nanoshells, carbon and silica nanomaterials have been employed for PTT treatment of cancer.[105-107] The basic demand for potential use of PTT is the excellent targeting ability of photoabsorbers to tumors, which can improve the therapeutic efficacy while reduce the side effects. For localizing tumors, understanding the distribution of photoabsorbers in tumors, and assessing the therapeutic efficacy, imaging tools are also needed.[108,109] UCNP-based cancer therapies, particularly NIR-light induced PTT which has been demonstrated by several *in vitro* and *in vivo* experiments,[110-113] could be useful theranostic tools for various kinds of tumors.

In 2011, Song and coworkers fabricated novel UCNPs@Ag core-shell nanocomposites for the integrated UCL imaging and PTT of cancer cells.[114] Hexagonal $NaYF_4$: Yb, Er UCNPs were prepared to act as efficient NIR-to-visible materials for UCL imaging. Ag nanoshell with a thickness of 6-8 nm and adjusted

surface plasma resonance (SPR) absorption at 980 nm was coated on the surface of UCNPs to provide photothermal effect, such nanocomposites showed good dispersibility and photochemical stability in aqueous solution. Compared with the bared UCNPs, Ag shell coated UCNPs showed efficient thermal effect in aqueous solution beyond the inflexion irradiation power at 1.12×10^5 W/cm^2. The PTT effect of UCNPs@Ag was estimated through the NIR irradiation of HepG2 and BCap-37 cells with a 980 nm laser (1.5 W/cm^2), after 20 min of irradiation, the viability of the HepG2 and BCap-37 cells were remarkably reduced to 4.62% and 5.43%, respectively. The irradiation power could be much lower (1.5 W/cm^2) than that reported for Au nanoshells or nanorods,[115,116] which can be attributed to the greater concentration of UCNPs@Ag on the surface of cells or the larger absorption cross-section of the Ag shell. Moreover, UCNPs@Ag could play an important role to localize the cancer and detect thermal variation of the abnormal area in the PTT process due to its UCL imaging ability. This UCNPs based nanocomposites provide potential nanoplatform for diagnostic, tracing and imaging guided PTT of cancer.

In another experiment, through the layer-by-layer assembly method, Cheng et al. proposed an uncomplicated synthesis procedure of multifunctional nanoparticles (MFNPs) for UCL/MR dual-imaging guided PTT of tumors.[105] Such MFNPs are consist of UCNPs as the internal core to provide efficient UCL emission, an intermediate layer of ultra-small iron oxide nanoparticles (IONPs) to render such MFNPs superparamagnetic, and a outermost shell of gold that possesses strong NIR absorption to provide the photo-thermal effect.[117] PEG-functionalized MFNPs (MFNP-PEG) primarily accumulate in the tumor region, as been demonstrated by UCL and T2-weighted MR imaging. *In vivo* PTT studies were conducted with 4T1 tumor bearing mice, the surface temperature of tumors in experiment group (MFNP-PEG + magnetic field + 808 nm laser) increased remarkably to 50 ^{o}C. After 2 days of treatment, the tumor in experimental group disappeared and no tumor re-growth was observed over a period of 40 days, while in all of the control groups, the tumors kept rapid growing and all the mice died within 18 days. Histological analysis indicated that although MFNP-PEG tended to retain for a relatively long

period, no obvious toxic effect can be observed to mice. Furthermore, compared with several PTT experiments that used gold nanomaterials, the dose of gold (1.6 mg/kg) and the laser power (1 W/cm^2) applied in this experiment were much lower, which can be attributed to the enhanced accumulation of MFNP-PEG in the tumor under the magnetic field. For future cancer theranostic application, such nanocomposites should be further optimized to prolong the circulation half-time and reduce the internal retention and latent toxicity.

Alike the up-mentioned experiment, Liu et al. developed anti-HER2-conjugated MFNPs with the same core-shell structure of UCNP@Fe_3O_4@Au by the layer-by-layer assembling approach for biomarker-based cancer detection and simultaneous localized PTT of cancer cells (Fig. 8A).[54] MFNPs were modified with PEG and conjugated with anti-HER2-antibody to improve its dispersibility in aqueous solution as well as tumor-targeting ability. Anti-HER2-conjugated MFNPs were incubated with both HER2 positive BT474 and HER2 negative HeLa cells to demonstrate its targeting specificity. Intense UCL signals can be observed on the surface of BT474 cells under a 980 nm laser due to the affinity binding at the interface of MFNPs and BT474 cells, while only negligible signals was noticed in HeLa cells samples. Meanwhile, bare MFNPs also lacked binding affinity with HER2-positive cancer cells. For *in vitro* PTT experiments, both the BT474 and HeLa cells were incubated with anti-HER2-conjugated MFNPs under low temperature (4 ^oC for 1h) to reduce energy-dependent cell endocytosis of MFNPs. Under the 808 nm irradiation, remarkable cell killing effect can be observed only in the BT474 cells group, as shown in Fig. 8B, indicating the localized PTT effect of anti-HER2-conjugated MFNPs. Interestingly, a small amount of BT474 cells adjacent to those dead cells were noticed to evade the PTT effect of anti-HER2-conjugated MFNPs, which can be attributed to the inherent heterogeneity of tumor cells. Compared with earlier reported localized PTT defined with laser spot sizes,[118] such nanocomposites can be useful phototheranostic tools for tumor detection and high-precision localized PTT of cancer in the future.

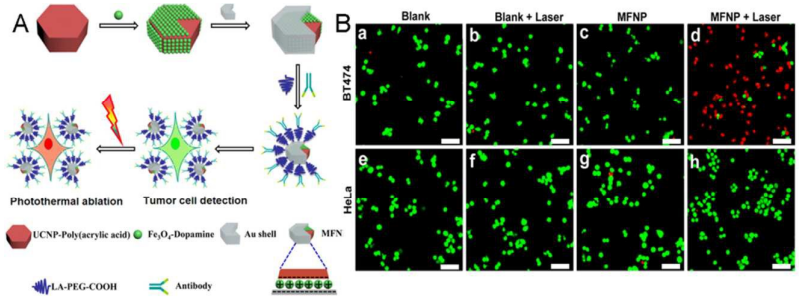

Fig. 8 (A) Schematic Illustration of the Synthesis Procedure of Anti-HER2-Conjugated MFNPs. (B) Images showing the living/dead status of cancer cells after PTT in the conditions as specified, including multiple control experiments. (Adapted with permission from ref. 54. Copyright 2014, American Chemical Society).

Accordingly, well-defined UCNPs based MFNPs can be promising platforms for imaging-guided tumor detection and localized PTT, especially UCNPs coupled with plasmonic nanomaterials that possess strong absorption in the NIR region. Future efforts should be devoted to the fabrication of novel nanocomposites that are easily handled, moreover, higher therapeutic effect and less toxicity are two of the prerequisites for clinical applications.

4.3 Synergistic cancer therapeutics

UCNPs based single modality phototherapy has attracted tremendous attention and has made enormous achievements. Except PDT and PTT, UCNPs can be also applied to photo-based drug delivery for chemo- and radio- therapy as well as gene therapy for cancer. The combination of UCNPs based PDT/PTT and other therapeutic strategies could give synergistic and enhanced treatment efficacy compared with single modality therapy. Abundant efforts have been devoted to this realm to seek for more convenient and efficient therapeutic strategies for cancer and other diseases that threatened our health.

Liu's group have made great efforts for UCNPs based synergistic cancer therapeutics, for instance, in 2014, they have prepared protein (bovine serum albumin,

BSA) coated UCNPs that loaded with Rose Bengal (RB) and IR825 (an NIR absorption dye) for imaging guided synergistic PDT and PTT of cancer (see Fig. 9a).[119] $NaGdF_4$: Yb, Er naocrystals were synthesized and modified with polyacrylic acid (PAA) and further conjugated with BSA *via* the formation of amide bonds. As-prepared UCNPs@BSA exhibited noticeable dispersibility in both water and PBS buffer with enhanced physiological stability. Rose Bengal can be excited by the green emission (540 nm) of UCNPs due to the well overlapped characterized bands between them, thus under a 980 nm excitation, such nanocomposites are able to produce singlet oxygen and perform effective PDT for cancer cells. Furthermore, the dual-loaded IR 825 is able to induce hyperthermia of cancer cells under a 808 nm excitation without affect the red emission and the 980 nm excitation of UCNPs. As been demonstrated by *in vitro* experiments, remarkable cell viability decrease can be observed under a 980 nm excitation. Meanwhile, PTT caused by 808 nm excitation possesses slight higher cell killing ability than PDT caused by UCNPs under the 980 nm excitation. Furthermore, under the combined irradiation of 980 nm and 808 nm NIR lasers, UCNP@BSA-RB& IR825 could result in much lower cell viability than single PDT or PTT, indicating the synergistic treatment effect of two therapeutic strategies. *In vivo* experiments with 4T1 tumor bearing mice were also conducted by intratumorally (i.t.) injected with UCNP@BSA-RB& IR825. Since the existence of Gd doping, such nanocomposite can also act as UCL/T1-MR dual-modal imaging agents, as shown in Fig. 9b and 9c. Obvious temperature rise (from ~ 30 ^{o}C to ~ 45 ^{o}C) in tumor region can be captured by IR thermal camera upon 5 min irradiation under 808 nm (0.35 W/cm^2) laser after i.t. injection with UCNP@BSA-RB& IR825 indicating the existence of PTT effects, while 980 nm excitation did not cause any temperature increase in the same period of time. After 14 days of synergistic PDT and PTT, the tumor growth was remarkably inhibited compared with mono-therapy and control groups, indicating the superior therapeutic efficacy of combined treatment. Such UCNPs based nanocomposites act as cancer phototheranostic agents with elevated therapeutic efficacy than traditional mono-therapy strategies (see Fig. 9d). Moreover, unlike the utilize of noble metal coated UCNPs for PTT, such

nanocomposites did not caused the compromise of overall fluorescent emission of UCNPs, thus they were more favorable for imaging-guided therapy.

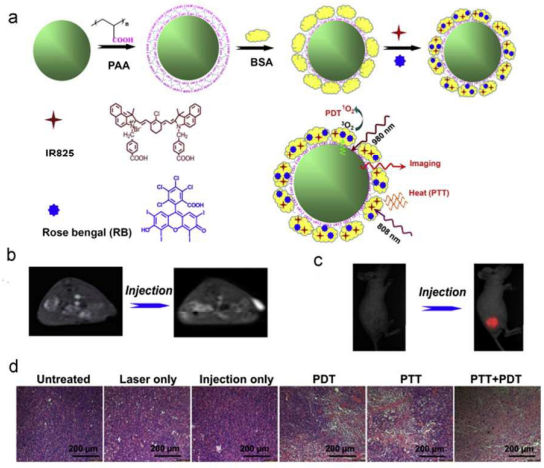

Fig. 9 (a) A schematic illustration to show the synthesis of UCNP@BSA-RB& IR825 nanocomplex, as well as the mechanism of both PDT and PTT therapies based on this system. (b) and UCL images (c) of mice before and after intratumoral injection with UCNP@BSA-RB& IR825. (d) Micrographs of H&E-stained tumor slices harvested from mice with different treatments indicated. (Adapted with permission from ref. 119. Copyright 2014, Elsevier).

In another experiment, for the first time, the same group took advantage of UCNPs conjugated with Ce6 and small interfering RNA (siRNA) to achieve synergistic therapeutic effect for cancer cell killing.[61] $NaGdF_4$: Yb, Er UCNPs were synthesized through thermal decomposition method and coated with PEG@2×PEI through layer-by-layer method, and the nanoparticles were further loaded with Ce6 and Polo-like kinase 1 (Plk1) siRNA, as shown in Fig. 10a. Under a 980 nm excitation, UCNPs can emit red light to excite Ce6 and produce cytotoxic singlet oxygen to kill cancer cells. While the Plk1 siRNA is able to silence Plk1 which is crucial in DNA replication and is overexpressed in various kinds of cancer cells, and the silence of Plk1 will finally cause cell apoptosis. Confocal fluorescence microscope demonstrates the existence of both UCL signals and fluorescence signals from Ce6 and fluorescently labeled siRNA, suggesting the successful cell uptake of such nanocomposites. Western blotting experiments indicate that cancer cells treated with UCNP-PEG@2 × PEI-Ce6-siPlk1 remarkably inhibits Plk1 expression (see Fig. 10b).

In vitro synergistic PDT/gene therapy was conducted with HeLa cells. Compared with single treatment (PDT or gene therapy alone), combined PDT and gene therapy for cancer cells treated with UCNP-PEG@2 × PEI-Ce6-siPlk1 under a 980 nm excitation can bring much lower cell viability (see Fig. 10c). Furthermore, due to the well designed surface coating of UCNPs, such nanocomposites well act as siRNA vector even in serum. Meanwhile, due to the reserve of green emission (540 nm) of UCNPs, such nanocomposites also serve as imaging guided synergistic PDT/gene therapy agents for cancer theranostics.

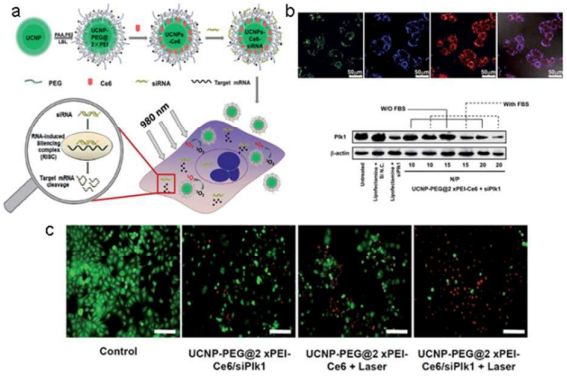

Fig. 10 (a) Schematic illustration showing the functionalization of UCNPs, co-loading with Ce6 and siRNA, and then the combined PDT and gene therapy delivered by UCNPs. (b) Confocal microscopy images of HeLa cells after incubation with UCNP–PEG@2 × PEI–Ce6–FAM-siRNA for 4 h. Western blotting results to determine Plk1 expression of HeLa cells after various treatments indicated. β-Actin was also detected as the internal control. (c) Fluorescence micrographs showing the calcein-AM (green, for living cells) and PI (red, for dead cells) double stained HeLa cells. Scale bar: 100 mm. (Adapted with permission from ref. 61. Copyright 2014, Royal Society of Chemistry).

Very recently, Lin et al. constructed a novel nanoplatform based on mesoporous silica coated UCNPs which were further conjugated with PS molecules $Au_{25}(SR)_{18}$ clusters and a kind of pH/temperature sensitive polymer P(NIPAm-MAA) as well as doxorubicin (DOX) (denoted as YSAP-DOX) for imaging-guided PDT/PTT/chemo tri-modality therapy of cancer.[120] Core-shell Y_2O_3:Yb,Er@Y_2O_3:Yb UCNPs were synthesized and modified with mesoporous silica to improve its dispersibility in water. Further processed with APTES renders such UCNPs positively charged, thus they are

able to conjugate with negative charged $Au_{25}(SR)_{18}$ through electrostatic interactions. $Au_{25}(SR)_{18}$ clusters can act as photodynamic/photothermal dual-modality therapy agents after receiving energy transformed from UCNPs under 980 nm laser excitation. Meanwhile, due to the relative lower pH values of cancer cells, as well as the elevated temperature induced by PTT, the pH/temperature sensitive polymer P(NIPAm-MAA) is able to act as an intelligent switch to achieve targeted and controlled release of DOX in cancer cells to improve its therapeutic efficiency. After intravenously injection of YSAP-DOX to H22 tumor bearing mice, the therapeutic effect was evaluated under the treatment with NIR excitation light. Compared with control groups, *i.e.*, without any NIR excitation or YSAP-UCNPs groups without DOX loading, the growth of tumor was remarkably inhibited with a size of only 6.7 mm while the size of tumor in control groups ranged from 16 mm to 28.6 mm, indicating the synergistic and elevated therapeutic efficiency of YSAP-DOX under NIR excitation. Meanwhile, body weight and histological analysis of kidney, spleen, lung, heart, and liver of the mice revealed no obvious adverse effect or organ damage from such nanocomposites. Furthermore, due to the Er and relative large amount of Y/Yb doping in UCNPs, such nanocomposites can also be applied to *in vivo* UCL/CT bimodal imaging of tumor.

As been summarized above, UCNPs base nanocomposites can not only applied for single modality therapy, but also compatible for the synergistic and multi-modality cancer treatment.[121-124] Meanwhile, because of the intrinsic properties of UCNPs, besides the therapeutic capacity, such nanocomposites are generally suitable for multi-modal imaging for cancer cells or tumor tissue, and also promising carriers for photo-induced drug delivery,[125-127] thus they are highly significant and meaningful to be explored as multifunctional nanoplatforms for cancer phototheranostics.

5. Biosafety of UCNPs

Because of the widespread use of UCNPs in biomedical applications, scientists had

never stopped their steps on biosafety evaluation of UCNPs. Plenty of *in vitro* and *in vivo* researches have been completed within recent years. Since it has been comprehensively discussed in several recent reviews,[8,128] herein, we will have a brief summarization and discussion of the recent works in terms of biosafety evaluation of UCNPs.

5.1 Toxicity of UCNPs

For potential cytotoxicity evaluation of UCNPs, the usual methods include MTT (methyl thiazolyl tetrazolium), MTS (3-(4,5-dimethylthiazol-2-yl)-5-(3-carboxymethoxyphenyl)-2-(4-sulfophenyl)-2H-tetrazolium, sodium salts), and CCK-8 assays assays are most widely used. As been summarized in Table 2, according to the literatures, UCNPs with different components, various size and different surfactant typically show rather weak cytotoxicity at high incubating concentration, in most cases, the viability of different cell lines usually keep more than 85%.

Table 2: Cytotoxicity evaluation of different UCNPs.

UCNPs	Surfacant	Size (nm)	Incubating concentration (μg/mL)	Incubating time (h)	Viability	Cell line	Ref
$NaYF_4$: Yb, Er	PEI	~130	3.125-200	24	>90%	L929	24
$NaYF_4$:Yb,Tm	PAA	39	0-600	24	>90%	HeLa	129
$NaYF_4$:Yb,Er,Tm	PEG-RGD	~14	0.1-1000	24	>85%	U87MG	75
$LiYF_4$:Yb,Er	SDS	17-20	200	24	~100%	L929	130
$NaGdF_4$:Yb,Er	EDTA	~100	0-500	36	>85%	GES-1	131
$NaLuF_4$:Yb,Er,Tm	GdDTPA	80-100	800	24	~90%	HeLa	92
$NaYF_4$:Yb,Er@$NaGdF_4$	ANG, PEG	49.6-62.6	1000	24	~100%	HeLa	70
$NaYF_4$:Yb,Er,Tm@$NaGdF_4$	PEG	~30	1000	24	>80%	RAW264.7	132
Y_2O_3:Yb,Er	PEG	<200	1000	24	96%	HeLa	133
$NaYF_4$:Yb,Er@$mSiO_2$	PEG	22	400	24	~100%	L929	134
$NaYF_4$:Yb,Er@mSiO2	PEG-FA	~80	50	24	~80%	L929	135
$NaYF_4$:Yb,Tm@Fe_xO_y	Dopamine	30	100	48	>80%	KB	136

Toxicity evaluation of UCNPs in animal models has also been conducted by several groups in recent years. For instance, the long-term toxicity of UCNPs is

systematically investigated by Xiong et al. in 2010. In their experiment, mice are intravenously injected with PAA-UCNPs (11.5 nm, 15 mg/kg), the behavior, body weight, serum biochemistry, hematology and histology are observed and surveyed within 115 days. They found that compared with the control group, mice treated with PAA-UCNPs only existed small body weight difference, while had normal drinking and eating behavior, activity, neurological status and exploratory behavior. Moreover, histological analysis 115 days post-injection indicated PAA-UCNPs (15 mg/kg) did not induce any abnormal in organs including heart, lung, liver and kidney, only the spleen was slightly hyperplasia by treatment with PAA-UCNPs. Meanwhile, the blood smears from mice treated with PAA-UCNP indicated that the number and shape of red blood cells, platelets and white blood cells maintain normal. Total bilirubin and several important enzymes including aspartate aminotransferase, alanine aminotransferase also showed no obvious difference with control group.[137]

The toxicity of UCNPs has also been investigated in *Caenorhabditis elegans* and zebrafish models. Zhou et al. found in their experiment that C. elegans worms incubated with PEI-UCNPs and *Escherichia coli* (*E. coli*) showed no obvious difference on life span, egg production and viability, and growth rate with worms only treated with *E. coli*.[138] Take advantage of the zebrafish model, the *in vivo* toxicity of β-NaYF4:Ce,Tb UCNPs is investigated by Jang et al.[139] They indicated that the group treated with 500 pM of QDs showed significant smaller heart and the absence of looping in the embryos, i.e., the development of heart was delayed. While the group treated with UCNPs (500 pM) displayed similar morphology of heart with control group, only at much higher concentration (almost 10 times of QDs), the toxicity of UCNPs was noticeable.

Moreover, the phytotoxicity of UCNPs has also been investigated in the plant model. Yin and coworkers chose soybean as a model plant, and investigated the subchronic phytotoxicity, translocation and biotransformation of UCNPs.[140] They found that relative low concentration of UCNPs (10 μg/mL) led to growth promotion for roots and stems, while high concentration of UCNPs (exceed 10 μg/mL) had inhibition effect on the growth of plant during the subchronic incubation time for 22 d.

According to the UCL imaging and ICP-MS data analysis of soybean plant, they indicated that UCNPs can be absorbed by root and consequently transformed to stem and leaf through vascular bundles and kept stable within 10 days incubation. Although these above mentioned studies are confined in cells and living models, they can provided preliminary proof and impetus for further validation of biosafety of UCNPs.

5.2 Excretion of UCNPs

As another important issue in terms of the biosafety, research on the excretion of UCNPs has also attracted tremendous attention in recent years. The FDA rules that any agents injected into the human body, especially diagnostic agents, should be completely cleared in a reasonable amount of time.[141] Alike most of the clinical drugs, research of the clearance of UCNPs have focused on the hepatobiliary excretion and renal excretion systems. Xiong and coworkers indicated the biliary excretion of PAA-UCNPs by athymic nude mice model.[137] At seven days post-injection with 15 mg/kg UCNPs *via* the tail vein, UCL signals at the intestinal tract indicated that UCNPs are cleared through hepatobiliary transport. Importantly, at 21 days post-injection, UCL signals are only detected at the intestinal tract and maintained up to 90 days. After 115 days of injection, almost no signals of UCNPs could be detected in mice, indicating that most of the PAA-UCNPs in the body of mice have been excreted. While in another experiment recently, they[56] found that PEG-modified and ^{153}Sm-labeled UCNPs with a hydrophobic diameter of smaller than 10 nm, can be excreted from the body of mice through renal excretion. Using gamma counter detection, they noticed that UCNPs can be tracked from 0.5 h to 6 h post-injection in the bladder at a concentration of 5.28 ± 0.2%ID g^{-1}. Also, UCNPs could be observed in the large intestine 1 h post injection at a concentration of 0.21 ± 0.04%ID g^{-1}. They concluded that the size of UCNPs can affect the excretion of UCNPs and small-sized UCNPs can be eliminated from the body of mice through two routes simultaneously. Since the excretion of UCNPs is a complicated process, plenty of factors could affect the clearance of UCNPs, including the size and surfactant of UCNPs. For the sake of

further application of UCNPs in human body, abundant efforts need to be devoted to researches on the mechanisms and process of UCNPs excretion.

6. Conclusions and perspectives

UCNPs based nanocomposites have shown high potential to act as phototheranostic agents for cancer. As summarized above, the intrinsic properties render UCNPs suitable for bioimaging and many other biomedical applications including PDT, PTT and synergistic cancer therapeutics. However before it can be applied in clinical cancer phototheranostics, several challenges need to be well addressed.

Firstly, for the sake of *in vivo* application, the UCL efficiency needs further enhancement. Typically, the quantum yields of UCNPs are lower than 1%, which apparently cannot meet the requirement of clinical imaging and phototherapy. Thus, novel types of UCNPs with higher quantum yields need to be fabricated. For instance, core-shell structured UCNPs or separate activators from sensitizers in different layers would enhance the UCL efficiency remarkably, and novel host matrix like $NaLuF_4$ could also enhance the UCL efficiency. Meanwhile, UCNPs should be small enough (sub 10 nm) in order to be completely eliminated from body. They should be hydrophilic for achieving long-time circulation. Although surface modification could render UCNPs hydrophilic and relative long circulation time, for instance, PEG modified UCNPs usually have long blood circulation time, the luminescence efficiency is also compromised. Therefore, novel surfactants which render UCNPs water-dispersible while preserving the UCL efficiency are in urgent need.

Secondly, how to eliminate the influence of water and other components in blood to the UCNPs based phototheranostics needs to be duly handled. UCNPs are typically excited by 980 nm NIR light. Although it is located in the transparent window of tissue, water still has relative strong absorption at this wavelength. To resolve such a problem, novel sensitizers need to be well selected. For instance, the combined sensitizer group Nd-Yb which can be excited at 808 nm provides an alternative.

Furthermore, broad-band NIR-dyes act as antenna to sensitize UCNPs are also good options.[142]

Thirdly, the long-term biosafety of UCNPs needs to be carefully studied before they can be applied in clinic. Though it has been demonstrated in several *in vitro* and *in vivo* experiments that UCNPs are relatively biocompatible, it should be noticed that a long period (always weeks to months) is needed to completely eliminate residual UCNPs after intravenously or intratumorally injection. Although experimental dose of UCNPs demonstrates to have no obvious toxicity to cells or organisms, long-term residence of UCNPs would induce inevitable side-effects. Considering the toxicity of UCNPs may be dose-dependent, overdose of UCNPs would subsequently arouse serious adverse reaction. Therefore, the safe dosage of UCNPs needs further investigation.

Last but not least, systematic study of the *in vivo* uptake, circulation and elimination mechanisms of UCNPs is crucial for their safe clinical theranostic applications. Meanwhile, these fundamental researches provide significant information for individualized administration and further optimization of such UCNPs based phototheranostic nanocomposites.

Acknowledgements

We are grateful for the financial supports from National Natural Science Foundation of China (81271634), Doctoral Fund of Ministry of Education of China (No. 20120162110070), Hunan Provincial Natural Science Foundation of China (12JJ1012), and the Office of Science (BER), U.S. Department of Energy (DE-SC0008397).

References

1 V. Shanmugam, S. Selvakumar and C. S. Yeh, *Chem. Soc. Rev.*, 2014, **43**, 6254-6287.

2 M. C. Simões, J. J. Sousa and A. A. Pais, *Cancer Lett.*, 2015, **357**, 8-42.
3 G. Y. Chen, H. L. Qiu, Hailong Qiu, P. N. Prasad and X. Y. Chen, *Chem. Rev.*, 2014, **114**, 5161-5214.
4 C. Wang, L. Cheng and Z. Liu, *Theranostics*, **2013**, 3, 317-330.
5 E. de Boer, N. J. Harlaar, A. Taruttis, W. B. Nagengast, E. L. Rosenthal, V. Ntziachristos and G. M. van Dam, *Br. J. Surg.*, 2015, **102**, e56-e72.
6 H. Dong, S. R. Du, X. Y. Zheng, G. M. Lyu, L. D. Sun, L. D. Li, P. Z. Zhang, C. Zhang and C. H. Yan, *Chem. Rev.*, 2015, **115**, 10725-10815.
7 X. M. Li, F. Zhang and D. Y. Zhao, *Nano Today*, 2013, **8**, 643-676.
8 J. Zhou, Q. Liu, W. Feng, Y. Sun and F. Y. Li, *Chem. Rev.*, 2015, **115**, 395-465.
9 H. Dong, L. D. Sun and C. H. Yan, *Chem. Soc. Rev.*, 2015, **44**, 1608-1634.
10 Z. J. Gu, L. Yan, G. Tian, S. J. Li, Z. F. Chai and Y. L. Zhao, *Adv. Mater.*, 2013, **25**, 3758-3779.
11 W. Zeng, X. Wang, P. Xu, G. Liu, H. S. Eden and X. Chen, *Theranostics*, 2015, **5**, 559-582.
12 S. Wang, X. Wang, X. Chen, X. Cao, J. Cao, X. Xiong and W. Zeng, *RSC Adv.*, 2016, **6**, 46317-46324.
13 J. Wang, T. Wei, X. Y. Li, B. H. Zhang, J. X. Wang, C. Huang and Q. Yuan, *Angew. Chem. Int. Ed. Engl.*, 2014, **53**, 1616-1620.
14 G. Y. Chen, H. Ågren, T. Y. Ohulchanskyy and P. N. Prasad, *Chem. Soc. Rev.*, 2015, **44**, 1680-1713.
15 J. Zhou, Z. Liu and F. Y. Li, *Chem. Soc. Rev.*, 2012, **41**, 1323-1349.
16 W. Y. Yin, G. Tian, W. L. Ren, L. Yan, S. Jin, Z. J. Gu, L. J. Zhou, J. Li and Y. L. Zhao, *Dalton Trans.*, 2014, **43**, 3861-3870.
17 K. Wang, J. B. Ma, M. He, G. Gao, H. Xu, J. Sang, Y. X. Wang, B. Q. Zhao and D. X. Cui, *Theranostics*, 2013, **3**, 258-266.
18 G. Jalani, R. Naccache, D. H. Rosenzweig, S. Lerouge, L. Haglund, F. Vetrone and M. Cerruti, *Nanoscale*, 2015, **7**, 11255-11262.
19 A. Carlos Yanes, A. Santana-Alonso, J. Méndez-Ramos, J. del-Castillo and V. D. Rodríguez, *Adv., Funct., Mater.*, 2011, **21**, 3136-3142.
20 Q. Ju, D. T. Tu, Y. S. Liu, R. F. Li, H. M. Zhu, J. C. Chen, Z. Chen, M. D. Huang and X. Y. Chen, *J. Am. Chem. Soc.*, 2012, **134**, 1323-1330.
21 J. Wang, F. Wang, C. Wang, Z. Liu and X. G. Liu, *Angew. Chem. Int. Ed. Engl.*, 2011, **50**, 10369-10372.
22 P. Alonso-Cristobal, O. Oton-Fernandez, D. Mendez-Gonzalez, J. F. Díaz, E. Lopez-Cabarcos, I. Barasoain and J. Rubio-Retama, *ACS Appl. Mater. Interfaces*, 2015, **7**, 14992-14999.
23 M. He , P. Huang, C. L. Zhang, H. Y. Hu, C. C. Bao, G. Gao, R. He and D. X. Cui, *Adv., Funct., Mater.*, 2011 , **21**, 4470-4477.
24 J. Zhou, X. J. Zhu, M Chen, Y Sun and F. Y. Li, *Biomaterials*, 2012, **33**, 6201-6210.
25 Y. S. Liu, D. T. Tu, H. M. Zhu and X. Y. Chen, *Chem. Soc. Rev.*, 2013, **42**, 6924-6958.
26 F. Wang and X. G. Liu, *Acc. Chem. Res.*, 2014, **47**, 1378-1385.

27 F. Wang, Y. Han, C. S. Lim, Y. H. Lu, J. Wang, J. X, H. Y. Chen, C. Zhang, M. H. Hong and X. G. Liu, *Nature*, 2010, **463**, 1061-1065.
28 P. Y. Qiu, N. Zhou, H. Y. Chen, C. L. Zhang, G. Gao and D. X. Cui, *Nanoscale*, 2013, **5**, 11512-11525.
29 J. Shen, L. Zhao and G. Han, *Adv. Drug. Deliv. Rev.*, 2013, **65**, 744-755.
30 Y. M. Yang, *Mikrochim Acta.*, 2014, **181**, 263-294.
31 F. Wang, R. R. Deng and X. G. Liu, *Nat. Protoc.*, 2014, **9**, 1634-1644.
32 Z. Wang, C. H. Liu, L. J. Chang and Z. P. Li, *J. Mater. Chem.*, 2012, **22**, 12186-12192.
33 Da. Chen and Y. S. Wang, *Nanoscale*, 2013, **5**, 4621-4637.
34 G. Tian, Z. J. Gu, L. J. Zhou, W. Y. Yin, X. X. Liu, L. Yan, S. Jin, W. L. Ren, G. M. Xing, S. J. Li and Y. L. Zhao, *Adv. Mater.*, 2012, **24**, 1226-1231.
35 P. Ramasamy, P. Chandra, S. W. Rhee and J. Kim, *Nanoscale*, 2013, **5**, 8711-8717.
36 W. Y. Yin, L, N, Zhao, L. J. Zhou, Z. J. Gu, X. X. Liu, G. Tian, S. Jin, L. Yan, W. L. Ren, G. M. Xing and Y. L. Zhao, *Chemistry-A European Journal*, 2012, **18**, 9239-9245.
37 M. Y. Ding, Y. R. Ni, Y. Song, X. X. Liu, T. L. Cui, D. Q. Chen, Z. G. Ji, F. Xu, C. H. Lu, Z. Z. Xu, *J. Alloys. Compd.*, 2015, **623**, 42-48.
38 W. Y. Yin, G. Tian, W. L. Ren, L. Yan, S. Jin, Z. J. Gu, L. J. Zhou, J.Li and Y. L. Zhao, *Dalton Trans.*, 2014, **43**, 3861-3870.
39 Y. Hu, B. Wu, Q. Jin, X. Wang, Y. Li, Y. Sun, J. Huo and X. Zhao, *Talanta*, 2016, **152**, 504-512.
40 M. Wang, Y. Zhu and C. B. Mao, *Langmuir.*, 2015, **31**, 7084-7090.
41 E. M. Chan, G. Han, J. D. Goldberg, D. J. Gargas, A. D. Ostrowski, P. J. Schuck, B. C. Cohen and D. J. Milliron, *Nano Lett.*, 2012, **12**, 3839-3845.
42 V. Muhr, S. Wilhelm, T. Hirsch and O. S. Wolfbeis, *Acc. Chem. Res.*, 2014, **47**, 3481-3493.
43 Z. G. Chen, H. L. Chen, H. Hu, M. X. Yu, F. Y. Li, Q. Zhang, Z. G. Zhou, T. Yi and C. H. Huang, *J. Am. Chem. Soc.*, 2008, **130**, 3023-3029.
44 H. P. Zhou, C. H. Xu, W. Sun and C. H. Yan, *Adv. Funct. Mater.*, 2009, **19**, 3892-3900.
45 H. Hu, M. X. Yu, F. Y. Li, Z. G. Chen, X. Gao, L. Q. Xiong and C. H. Huang, *Chem. Mater.*, 2008, **20**, 7003-7009.
46 Y. Cen, Y. M. Wu, X. J. Kong, S. Wu, R. Q. Yu and X. Chu, *Anal. Chem.*, 2014, **86**, 7119-7127.
47 G. S. Yi and G. M. Chow, *Chem. Mater.*, 2007, **19**, 341-343.
48 S. S. Cui, D. Y. Yin, Y. Q. Chen, Y. F. Di, H. Y. Chen, Y. X. Ma, S. Achilefu and Y. Q. Gu, *ACS Nano*, 2013, **7**, 676-688.
49 W. L. Ren, G. Tian, S. Jian, Z. J. Gu, L. J. Zhou, L. Yan, S. Jin, W. Y. Yin and Y. L. Zhao, *RSC Advances*, 2012, **2**, 7037-7041.
50 G. Tian, W. Y. Yin, J. J. Jin, X. Zhang, G. M. Xing, S. J. Li, Z. J. Gu and Y. L. Zhao, *J. Mater. Chem. B*, 2014, **2**, 1379.
51 S. Jin, L. J. Zhou, Z. J. Gu, G. Tian, L. Yan, W. L. Ren, W. Y. Yin, X. D. Liu, X. Zhang, Z. B. Hu and Y. L. Zhao, *Nanoscale*, 2013, **5**, 11910-11918.

52 H. J. Wang, C. H. Dong, P. Q. Zhao, S. Wang, Z. Y. Liu, J. Chang, *Int. J. Pharm.*, 2014, **466**, 307-313.
53 W. P. Fan, W. B. Bu, Z. Zhang, B. Shen, H. Zhang, Q. J. He, D. L. Ni, Z. W. Cui, K. L. Zhao, J. W. Bu, J. L. Du, J. N. Liu and J. L. Shi, *Angew. Chem. Int. Ed. Engl.*, 2015, **127**, 14232-14236.
54 J. W. Shen, K. Y. Li, L. Cheng, Z. Liu, S. T. Lee and J. Liu, *ACS Appl. Mater. Interfaces*, 2014, **6**, 6443-6452.
55 X. K. Jia, J. J. Yin, D. G. He, X. X. He, K. M. Wang, M. Chen, Y. H. Li, *J. Biomed. Nanotechnol.*, 2013, **9**,2063-2072.
56 T. Y. Cao, Y. Yang, Y. Sun, Y. Q. Wu, Y. Gao, W. Feng, F. Y. Li, *Biomaterials*, 2013, **34**, 7127-7134.
57 Q. T. Chen, X. Wang, F. H. Chen, Q. B. Zhang, B. Dong, H. Yang, G. X. Liu and Y. M. Zhu, *J. Mater. Chem.*, 2011, **21**, 7661-7667.
58 F. Wang, R. R. Deng, J. Wang, Q. X. Wang, Y. Han, H. M. Zhu, X. Y. Chen and X. G. Liu, *Nat. Mater.*, 2011, **10**, 968-973.
59 A. G. Dong, X. C. Ye, J. Chen, Y. J. Kang, T. Gordon, J. M. Kikkawa and C. B. Murray, *J. Am. Chem. Soc.*, 2011, **133**, 998-1006.
60 A. Sedlmeier and H. H. Gorris, *Chem. Soc. Rev.*, 2015, **44**, 1526-1560.
61 X. Wang, K. Liu, G. B. Yang, L. Cheng, L. He, Y. M. Liu, Yo. G. Li, L. Guo and Z. Liu, *Nanoscale*, 2014, **6**, 9198-9205.
62 H. Q. Chen, F. Yuan and L. Wang, *Anal. Methods*, 2013, **5**, 2873-2879.
63 N. M. Idris, M. K. Gnanasammandhan, J. Zhang, P. C. Ho, R. Mahendran and Y. Zhang, *Nat. Med.*, 2012, **18**, 1580-1585.
64 S. Q. He, K. Krippes, S. Ritz, Z. J. Chen, A. Best, H. J. Butt, V. Mailänderab and S. Wu, *Chem. Commun.*, 2015, **51**, 431-434.
65 L. L. Fedoryshin, A. J. Tavares, E. Petryayeva, S. Doughan and U. J. Krull, *ACS Appl. Mater. Interfaces*, 2014, **6**, 13600-13606.
66 T. C. Ma, Y. Ma, S. J. Liu, L. L. Zhang, T. S. Yang, H. R. Yang, W. Lv, Q. Yu, W. J. Xu, Q. Zhao and W. Huang, *J. Mater. Chem. C*, 2015, **3**, 6616-6620.
67 Y. S. Liu, D. T. Tu, H. M. Zhu, E. Ma and X. Y. Chen, *Nanoscale*, 2013, **5**, 1369-1384.
68 Y. I. Park, K. T. Lee, Y. D. Suh and T. Hyeon, *Chem. Soc. Rev.*, 2015, **44**,1302-1317.
69 J. B. Ma, P. Huang, M. He, L. Y. Pan, Z. J. Zhou, L. L. Feng, G. Gao and Daxiang Cui, *J. Phys. Chem. B,* 2012, **116**, 14062-14070.
70 J. N. Liu, W. B. Bu, L. M. Pan, S. J. Zhang, F. Chen, L. P. Zhou, K. L. Zhao, W. J. Peng and J. L. Shi, *Biomaterials*, 2012, **33**, 7282-7290.
71 D. F. Peng, Q. Ju, X. Chen, R. H. Ma, B. Chen, G. X. Bai, J. H. Hao, X. S. Qiao, X. P. Fan and F. Wang, *Chem. Mater.*, 2015, **27**, 3115-3120.
72 F. Wang, X. G. Liu, *J. Am. Chem. Soc.*, 2008, **130**, 5642-5643.
73 F. Wang, X. G. Liu, *Acc. Chem. Res.*, 2014, **47**, 1378-1385.
74 W. B. Hu , X. M. Lu, R. C. Jiang, Q. L. Fan, H. Zhao, W. X. Deng, L. Zhang, L. Huang and W. Huang, *Chem. Commun.*, 2013, **49**, 9012-9014.
75 L. Q. Xiong, Z. G. Chen, Q. W. Tian, T. Y. Cao, C. J. Xu and F. Y. Li, *Anal. Chem.*,

2009, **81**, 8687-8694.
76 Q. Q. Zhan, J. Qian, H. J. Liang, G. Somesfalean, D. Wang, S. L. He, Z. G. Zhang and S. Andersson-Engels, *ACS Nano*, 2011, **5**, 3744-3757.
77 Y. F. Wang, G. Y. Liu, L. D. Sun, J. W. Xiao, J. C. Zhou and C. H. Yan, *ACS Nano*, 2013, **7**, 7200-7206.
78 L. V. Wang and S. Hu, *Science*, 2012, 335, 1458-1462.
79 F. Vetrone, R. Naccache, A. Juarranz de la Fuente, F. Sanz-Rodríguez, A. Blazquez-Castro, E. M. Rodriguez, D. Jaque, J. G. Solé and J. A. Capobianco, *Nanoscale*, 2010, **2**, 495-498.
80 J. N. Liu, W. B. Bu, L. M. Pan and J. L. Shi, *Angew. Chem. Int. Ed. Engl.*, 2013, **52**, 4375-4379.
81 S. K. Maji, S. Sreejith, J. Joseph, M. J. Lin, T. C. He, Y. Tong, H. D. Sun, S. W. Yu and Y. L. Zhao, *Adv. Mater.*, 2014, **26**, 5633-5638.
82 V. K. Tikhomirov, K. Driesen, V. D. Rodriguez, P. Gredin, M. Mortier and V. V. Moshchalkov, *Opt. Express.*, 2009, **17**, 11794-11798.
83 H. Y. Xing, W. B. Bu, S. J. Zhang, X. P. Zheng, M. Li, F. Chen, Q. J. He, L. P. Zhou, W. J. Peng, Y. Q. Hua and J. L. Shi, *Biomaterials*, 2012, **33**, 1079-1089.
84 F. Chen, W. B. Bu, S. J. Zhang, X. H. Liu, J. N. Liu, H. Y. Xing, Q. F. Xiao, L. P. Zhou, W. J. Peng, L. Z. Wang and J. L. Shi, *Adv. Funct. Mater.*, 2011, **21**, 4285-4294
85 Y. L. Liu, K. L. Ai, J. H. Liu, Q. H. Yuan, Y. Y. He and L. H. Lu, *Angew. Chem. Int. Ed. Engl.*, 2012, **51**, 1437-1442.
86 X. Q. Ge, L. Dong, L. N. Sun, Z. M. Song, R. Y. Wei, L. Y. Shi and H. G. Chen, *Nanoscale*, 2015, **7**, 7206-7215.
87 C. Chen, N. Kang, T. Xu, D. Wang, L. Ren and X. Q. Guo, *Nanoscale*, 2015, **7**, 5249-5261.
88 B. Liu, C. X. Li, P. A. Ma, Y. Y. Chen, Y. X. Zhang, Z. Y. Hou, S. S. Huang and J. Lin, *Nanoscale*, 2015, **7**, 1839-1848.
89 D. L. Ni, J. W. Zhang, W. B. Bu, H. Y. Xing, F. Han, Q. F. Xiao, Z. W. Yao, F. Chen, Q. J. He, J. N. Liu, S. J. Zhang, W. P. Fan, L. P. Zhou, W. J. Peng and J. L. Shi, *ACS Nano*, 2014, **8**, 1231-1242.
90 Z. Liu, Z. H. Li, J. H. Liu, S. Gu, Q. H. Yuan, J. S. Ren and X. G. Qu, *Biomaterials*, 2012, **33**, 6748-6757.
91 G. Tian, X. P. Zheng, X. Zhang, W. Y. Yin, J. Yu, D. L. Wang, Z. P. Zhang, X. L. Yang, Z. J. Gu and Y. L. Zhao, *Biomaterials*, 2015, **40**, 107-116.
92 J. Zhou, X. J. Zhu, M. Chen, Y. Sun and F. Y. Li, *Biomaterials*, 2012, **33**, 6201-6210.
93 L. Wang, J. H. Liu, Y. L. Dai, Q. Yang, Y. X. Zhang, P. P. Yang, Z. Y. Cheng, H. Z. Lian, C. X. Li, Z. Y. Hou, P. A. Ma and J. Lin, *Langmuir*, 2014, **30**, 13042-13051.
94 S. H. Tang, J. N. Wang, C. X. Yang, L. X. Dong, D. L. Kong and X. P. Yan, *Nanoscale*, 2014, **6**, 8037-8044.
95 G. Tian, W. Y. Yin, J. J. Jin, X. Zhang, G. M. Xing, S. J. Li, Z. J. Gu and Y. L. Zhao, *J. Mater. Chem. B*, 2014, **2**, 1379-1389.

96 Z. Liu, K. Dong, J. H. Liu, X. L. Han, J. S. Ren and X. G. Qu, *Small*, 2014, **10**, 2429-2438.
97 D. L. Ni, W. B. Bu, S. J. Zhang, X. P. Zheng, M. Li, H. Y. Xing, Q. F. Xiao, Y. Y. Liu, Y. Q. Hua, L. P. Zhou, W. J. Peng, K. L. Zhao and J. L. Shi, *Adv. Funct. Mater.*, 2014, **24**, 6613-6620.
98 J. H. Lee, T. S. Lee, J. Y. Ryu, S. Hong, M. Kang, K. B. Im, J. H. Kang, S. M. Lim, S. Park and R. Song, *J. Nucl. Med.*, 2013, **54**, 96-103.
99 Y. Sun, X. J. Zhu, J. J. Peng and F. Y. Li, *ACS Nano*, 2013, **7**, 11290-11300.
100 J. Zhou, M. X. Yu, Y. Sun, X. Z. Zhang, X. J. Zhu, Z. H. Wu, D. M. Wu and F. Y. Li, *Biomaterials*, 2011, **32**, 1148-1156.
101 Q. Liu, Y. Sun, C. G. Li, J. Zhou, C. Y. Li, T. S. Yang, X. Z. Zhang, T. Yi, D. M. Wu and F. Y. Li, *ACS Nano*, 2011, **5**, 3146-3157.
102 J. Rieffel, F. Chen, J. Kim, G. Chen, W. Shao, S. Shao, U. Chitgupi, R. Hernandez, S. A. Graves, R. J. Nickles, P. N. Prasad, C. Kim C, W. B. Cai and J. F. Lovell, *Adv. Mater.*, 2015, **27**, 1785-1790.
103 M. Wang, Z. Chen, W. Zheng, H. M. Zhu, S. Lu, E. Ma, D. T. Tu, S. Y. Zhou, M. D. Huang and X. Y. Chen, *Nanoscale*, **2014**, 6(14): 8274-8282.
104 F. J. Ai, Q. Ju, X. M. Zhang, X. Chen, F. Wang and G. Y. Zhu, *Sci. Rep.*, **2015**, 5: 10785.
105 L. Cheng, K. Yang, Y. G. Li, X. Zeng, M. W. Shao, S. T. Lee and Z. Liu, *Biomaterials*, 2012, **33**, 2215-2222.
106 Y. Wang, H. Wang, D. Liu, S. Song, X. Wang and H. Zhang, *Biomaterials*, 2013, **34**, 7715-7724.
107 H. Liu, D. Chen, L. Li, T. Liu, L. Tan, X. Wu and F. Tang, *Angew. Chem. Int. Ed. Engl.*, 2011, **123**, 921-925.
108 E. B. Dickerson, E. C. Dreaden, X. H. Huang, I. H. El-Sayed, H. H Chu, S. Pushpanketh, J. F. McDonald and M. A. El-Sayed, *Cancer Lett.*, 2008, **269**,57-66.
109 J. Kim, S. Park, J. E. Lee, S. M. Jin, J. H. Lee, I. S. Lee, I. Yang, J. S. Kim, S. K. Kim, M. H. Cho and T. Hyeon, *Angew. Chem. Int. Ed.*, 2006, **118**, 7918-7922.
110 J. Zhou, Y. Sun, X. Du, L.Xiong, H. Hua and F. Y. Li, *Biomaterials*, 2010, **31**, 3287-3295.
111 J. Zhou, M. X. Yu, Y. Sun, X. Z. Zhang, X. J. Zhu, Z. H. Wu, D. M. Wu and F. Y. Li, *Biomaterials*, 2011, **32**, 1148-1156.
112 C. Wang, H. Tao, L. Cheng and Z. Liu, *Biomaterials*, 2011, **32**, 6145-6154.
113 H. S. Qian, H. C. Guo, P. C. L. Ho, R. Mahendran and Y. Zhang, *Small*, 2009, **5**, 2285-2290.
114 B. Dong, S. Xu, J. Sun, S. Bi, D. Li, X. Bai, Y. Wang, L. P. Wang and H. W. Song, *J. Mater. Chem.*, 2011, **21**, 6193-6200.
115 L. R. Hirsch, R. J. Stafford, J. A. Bankson, S. R. Sershen, B. Rivera, R. E. Price, J. D. Hazle, N. J. Halas and J. L. West, *Proc. Natl. Acad. Sci. U. S. A.*, 2003, **100**, 13549-13554.
116 X. H. Huang , I. H. El-Sayed, W. Qian and M. A. El-Sayed, *J. Am. Chem. Soc.*, 2006, **128**, 2115-2120.
117 L. Cheng, K. Yang, Y. Li, J. Chen, C. Wang, M. Shao, S. T. Lee, and Z. Liu,

Angew. Chem. Int. Ed., 2011, **50**, 7385-7390.
118 L. Au, D. Zheng, F. Zhou, Z. Y. Li, X. Li and Y. Xia, *ACS Nano*, 2008, **2**, 1645-1652.
119 Q. Chen, C. Wang, L. Cheng, W. W. He, Z. P. Cheng and Z. Liu, *Biomaterials*, 2014, **35**, 2915-2923.
120 R. C. Lv, P. P. Yang, F. He, S. L. Gai, G. X. Yang, Y. L. Dai, Z. Y. Hou and J. Lin, *Biomaterials*, 2015, **63**, 115-127.
121 S. Yang, N. J. Li, Z. Liu, W. W. Sha, D. Y. Chen, Q. F. Xua and J. M. Lu, *Nanoscale*, 2014, **6**, 14903-14910.
122 G. X. Yang, R. C. Lv, F. He, F. Y. Qu, S. L. Gai, S. K. Du, Z. B. Wei and P. P. Yang, *Nanoscale*, 2015, **7**, 13747-13758.
123 W. P. Fan, B. Shen, W. B. Bu, F. Chen, Q. J. He, K. L. Zhao, S. J. Zhang, L. P. Zhou, W. J. Peng, Q. F. Xiao, D. L. Ni, J. N. Liu and J. L. Shi, *Biomaterials*, 2014, **35**,8992-9002.
124 Y. Y. Liu, Y. Liu, W. B. Bu, C. Cheng, C. J. Zuo, Q. F. Xiao, Y. Sun, D. L. Ni, C. Zhang, J. N. Liu and J. L. Shi, *Angew. Chem. Int. Ed. Engl.*, 2015, **54**, 8105-8109.
125 G. Liu, L. Zhou, Y. Su and C. M. Dong, *Chem. Commun.*, 2014, **50**, 12538-12541.
126 G. Tian, X. Zheng, X. Zhang, W. Yin, J. Yu, D. Wang, Z. Zhang, X. Yang, Z. Gu and Y. Zhao, *Biomaterials*, 2015, **40**, 107-116.
127 J. Lai, B. P. Shah, Y. Zhang, L. Yang and K. B. Lee, *ACS Nano*, 2015, **9**, 5234-5245.
128 Y. Sun, W. Feng, P. Yang, C. Huang and F. Li, *Chem. Soc. Rev.*, 2015, **44**, 1509-1525.
129 J. W. Shen, C. X. Yang, L. X. Dong, H. R. Sun, K. Gao and X. P. Yan, *Anal. Chem.*, 2013, **85**, 12166-12172.
130 D. Yang, Y. Dai, P. Ma, X. Kang, M. Shang, Z. Cheng, C. Li and J. Lin, *J. Mater. Chem.*, 2012, **22**, 20618.
131 G. Gao, C. Zhang, Z. Zhou, X. Zhang, J. Ma, C. Li, W. Jin and D. Cui, *Nanoscale*, 2013, **5**, 351-362.
132 Q. Xiao, W. Bu, Q. Ren, S. Zhang, H. Xing, F. Chen, M. Li, X. Zheng, Y. Hua, L. Zhou, W. Peng, H. Qu, Z. Wang, K. Zhao and J. Shi, *Biomaterials*, 2012, **33**, 7530-7539.
133 L. Dong, D. An, M. Gong, Y. Lu, H. L. Gao, Y. J. Xu and S. H. Yu, *Small*, 2013, **9**, 3235-3241.
134 C. Li, D. Yang, P. Ma, Y. Chen, Y. Wu, Z. Hou, Y. Dai, J. Zhao, C. Sui and J. Lin, *Small*, 2013, **9**, 4150-4159.
135 C. Li, Z. Hou, Y. Dai, D. Yang, Z. Cheng, P. Ma and J. Lin, *Biomater. Sci.*, 2013, **1**, 213.
136 A. Xia, Y. Gao, J. Zhou, C. Y. Li, T. S. Yang, D. M. Wu, L. M. Wu and F. Y. Li, *Biomaterials*, 2011, **32**, 7200-7208.
137 L. Q. Xiong, T. S. Yang, Y. Yang, C. J. Xu and F. Y. Li, *Biomaterials*, 2010, **31**, 7078-7085.
138 J. C. Zhou, Z. L. Yang, W. Dong, R. J. Tang, L. D. Sun and C. H. Yan, *Biomaterials*, 2011, **32**, 9059-9067.

139 G. H. Jang, M. P. Hwang, S. Y. Kim, H. S. Jang, K. H. Lee, *Biomaterials*, 2014, **35**, 440-449.
140 W. Yin, L. Zhou, Y. Ma, G. Tian, J. Zhao, L. Yan, X. Zheng, P. Zhang, J. Yu, Z. Gu and Y. Zhao, *Small*, 2015, **11**, 4774-4784.
141 H. S. Choi, W. Liu, P. Misra, E. Tanaka, J. P. Zimmer, B. Itty Ipe, M. G. Bawendi and J. V. Frangioni, *Nat. Biotechnol.*, 2007, **25**, 1165-1170.
142 W. Q. Zou, C. Visser, J. A. Maduro, M. S. Pshenichnikov and J. C. Hummelen, *Nat. Photonics*, 2012, **6**, 560-564.